The intracellular fate of zonula occludens 2 is regulated by the phosphorylation of SR repeats and the phosphorylation/*O*-GlcNAcylation of S257

Miguel Quiros[a], Lourdes Alarcón[a], Arturo Ponce[a], Thomas Giannakouros[b], and Lorenza González-Mariscal[a]

[a]Department of Physiology, Biophysics and Neuroscience, Center for Research and Advanced Studies (Cinvestav), Mexico City 07000, Mexico; [b]Department of Chemistry, Aristotele University of Thessaloniki, Thessaloniki 54621, Greece

ABSTRACT **Zona occludens 2 (ZO-2) has a dual localization. In confluent epithelia, ZO-2 is present at tight junctions (TJs), whereas in sparse proliferating cells it is also found at the nucleus. Previously we demonstrated that in sparse cultures, newly synthesized ZO-2 travels to the nucleus before reaching the plasma membrane. Now we find that in confluent cultures newly synthesized ZO-2 goes directly to the plasma membrane. Epidermal growth factor induces through AKT activation the phosphorylation of the kinase for SR repeats, serine arginine protein kinase 1, which in turn phosphorylates ZO-2, which contains 16 SR repeats. This phosphorylation induces ZO-2 entry into the nucleus and accumulation in speckles. ZO-2 departure from the nucleus requires intact S257, and stabilizing the β-*O*-linked *N*-acetylglucosylation (*O*-GlcNAc) of S257 with *O*-(2-acetamido-2-deoxy-D-glucopyranosylidene)amino-N-phenylcarbamate, an inhibitor of *O*-GlcNAcase, triggers nuclear exportation and proteosomal degradation of ZO-2. At the plasma membrane ZO-2 is not *O*-GlcNAc, and instead, as TJs mature, it becomes phosphorylated at S257 by protein kinase Cζ. This late phosphorylation of S257 is required for the correct cytoarchitecture to develop, as cells transfected with ZO-2 mutant S257A or S257E form aberrant cysts with multiple lumens. These results reveal novel posttranslational modifications of ZO-2 that regulate the intracellular fate of this protein.**

Monitoring Editor
Asma Nusrat
Emory University

Received: Apr 30, 2013
Revised: Jun 11, 2013
Accepted: Jun 17, 2013

INTRODUCTION

In epithelial cells, tight junctions (TJs) play a crucial role in regulating the movement of ions and molecules through the paracellular pathway and in maintaining a polarized distribution of proteins between the apical and basal membranes (for review see Gonzalez-Mariscal *et al.*, 2003). Zona occludens 2 (ZO-2) is a 160-kDa protein present at the cytoplasmic side of the TJ (Gumbiner *et al.*, 1991) and is made up of several domains and motifs (Jesaitis and Goodenough, 1994): the amino portion contains three PDZ domains, the middle section has an SH3 module and a guanylate kinase (GuK) domain, and the carboxyl region ends with the PDZ binding motif TEL and contains acidic and proline-rich domains that together constitute an actin-binding region (ABR).

ZO-2 functions as a scaffold that brings together multiple proteins at the TJ (for reviews see Fanning and Anderson, 2009; Gonzalez-Mariscal *et al.*, 2011). Thus the first PDZ domain associates to claudins; the second PDZ to ZO-1, to other ZO-2 proteins, and to the gap junction protein connexin 43; the third PDZ to JAMs; the SH3-GuK region, which is structured as a hinge, associates to the adherens junction protein α-catenin; the ABR region binds to actin, protein 4.1, and cingulin; and the TEL motif associates to Scribble, a member of the lateral membrane polarity complex.

This article was published online ahead of print in MBoC in Press (http://www.molbiolcell.org/cgi/doi/10.1091/mbc.E13-04-0224) on June 26, 2013.

Address correspondence to: Lorenza González-Mariscal (lorenza@fisio.cinvestav.mx).

Abbreviations used: bpNLS, bipartite nuclear localization signal; EGF, epidermal growth factor; MDCK, Madin–Darby canine kidney; NLS, nuclear localization signal; *O*-GlcNAc, β-*O*-linked *N*-acetylglucosylation; PKC, protein kinase C; PUGNAc, *O*-(2-acetamido-2-deoxy-D-glucopyranosylidene)amino-*N*-phenylcarbamate; SRPK, serine arginine protein kinase; TJ, tight junction; ZO-2, zona occludens 2.

The importance of ZO-2 in different tissues has been highlighted by the effect that its mutation, silencing, or overexpression exerts in humans, mice, and tissue cultures. In humans, mutation V48A localized in ZO-2's first PDZ domain, accompanied by a mutation in bile acid CoA, the enzyme that converts bile acids to their salt form, disrupts bile acid transport and circulation, leading to a hypercholanemia inherited disease. This suggests that ZO-2 stability is critical for the establishment of properly sealed TJs in hepatocytes (Carlton *et al.*, 2003). In humans, the genomic duplication of ZO-2 leads to overexpression of the protein and nonsyndromic hearing loss due to an increased expression of apoptosis genes in the hair cells of the inner ear, indicating a role of ZO-2 in the promotion of apoptosis (Walsh *et al.*, 2010). During mammalian development, ZO-2 knockout is lethal, stopping development in early gastrulation (Xu *et al.*, 2008). Studies with mouse chimeras showed that ZO-2 is crucial for the development of extraembryonic tissue and not for the embryo per se, although in adult mouse chimeras, the lack of ZO-2 reveals that the protein is essential for the establishment of the blood–testis barrier and male fertility (Xu *et al.*, 2009). In mouse EpH4 breast epithelial cells, ZO-2 silencing together with ZO-1 knockout inhibits claudin polymerization, whereas reexpression of either of these proteins reestablishes TJ formation, indicating a redundant role of these two ZO proteins in TJ strand formation (Tsukita *et al.*, 2009). ZO-2 silencing retards TJ formation induced by transfer of cultures from low to normal (1.8 mM) calcium-containing media and alters the cytoarchitecture of epithelial monolayers, widening the intercellular spaces and creating regions in the culture where cells grow on top of each other (Hernandez *et al.*, 2007).

Previously we found that ZO-2 has dual localization (Islas *et al.*, 2002). Thus in confluent cultures ZO-2 is found at TJs, whereas in sparse cultures it is also present in the nuclei distributed in speckles. ZO-2 associates with a variety of nuclear factors, including lamin B (Jaramillo *et al.*, 2004), the essential splicing factor SC35 (Islas *et al.*, 2002), the scaffold attachment factor B (SAF-B; Traweger *et al.*, 2003), and the transcription factors Jun, Fos, C/EBP (Betanzos *et al.*, 2004), Myc (Huerta *et al.*, 2007), and KyoT2 (Huang *et al.*, 2002). In addition, certain proteins enter the nucleus due to their association with ZO-2. Such is the case for the transcriptional coactivator YAP-2, which with its PDZ-binding motif binds to the first PDZ domain of ZO-2 (Oka *et al.*, 2010); the armadillo repeat protein deleted in velocardio-facial syndrome, whose PDZ-binding motif binds to the amino segment of ZO-2 containing the three PDZ domains (Kausalya *et al.*, 2004); and LIM and SH3-domain protein 1, whose SH3 domain binds the proline-rich region of ZO-2 (Mihlan *et al.*, 2012).

The intracellular traffic of ZO-2 is regulated by the cell cycle, as ZO-2 enters the nucleus at late G1 and departs during mitosis, thus explaining why no nuclear ZO-2 is observed in confluent quiescent cultures, whereas it is present in sparse, proliferating cells (Tapia *et al.*, 2009). ZO-2 nucleocytoplasmic shuttling is mediated by nuclear localization signals (NLSs) and nuclear exportation signals (NESs). Canine ZO-2 (cZO-2) sequence contains four NESs, two located at PDZ-2 and two at the GuK domain (Gonzalez-Mariscal *et al.*, 2006). Previously we demonstrated that these four NESs are functional and that the phosphorylation of S369 located within ZO-2 NES-1 by protein kinase Cε (PKCε) is critical for the exportation of the protein (Chamorro *et al.*, 2009). cZO-2 sequence contains three putative NLSs: two bipartite (bpNLS-$1_{83\text{-}98}$ and bpNLS-$2_{246\text{-}262}$) and one monopartite ($mpNLS_{185\text{-}188}$) located at linker U2 present between PDZ-1 and PDZ-2 (Jaramillo *et al.*, 2004). In addition, ZO-2 linker U2 contains 16 SR repeats (Jaramillo *et al.*, 2004). These motifs have been described in a variety of proteins (Boucher *et al.*, 2001), including transcriptional activators (Puigserver *et al.*, 1998; Lai *et al.*, 1999), and in a large family of eukaryotic pre-mRNA splicing factors called SR proteins (Valcarcel and Green, 1996). SR motifs are considered necessary and sufficient for targeting proteins to nuclear speckles and constitute the only sequence that is shared by all splicing factors that localize to speckles (Hedley *et al.*, 1995).

Here we analyze the effect that posttranslational modifications have on the intracellular fate of ZO-2 and observe that entry of ZO-2 into the nucleus and accumulation in speckles is regulated by the phosphorylation of its SR repeats by serine arginine protein kinase 1, through a process initiated by epidermal growth factor (EGF) activation of AKT. The β-*O*-linked *N*-acetylglucosylation (*O*-GlcNAc) of S257 at the nucleus favors the nuclear exportation of ZO-2, whereas the maturation of TJs is accompanied by ZO-2 phosphorylation at S257 by PKCζ.

RESULTS

In confluent epithelial monolayers ZO-2 does not travel to the nucleus

Here we analyzed whether in confluent monolayers newly synthesized ZO-2 travels to the nucleus. To detect the presence of ZO-2 at the nucleus, we blocked the nuclear exportation of this protein by incubating Madin–Darby canine kidney (MDCK) cells for 24 h with εv1-2, a PKCε permeable inhibitor peptide (Liedtke *et al.*, 2002), since we previously demonstrated that the nuclear exportation of ZO-2 requires the phosphorylation by PKCε of S369 located within NES-1 (Chamorro *et al.*, 2009). Figure 1 shows, as previously reported (Islas *et al.*, 2002), that ZO-2 is present in the nucleus of control monolayers in a sparse culture condition but not in confluent cultures. Blocking the nuclear exportation of ZO-2 with εv1-2 does not concentrate ZO-2 at the nucleus of confluent monolayers, indicating that in confluent cultures ZO-2 does not travel to the nucleus. Instead, strong increase in nuclear ZO-2 was observed in sparse cultures treated with εv1-2, and no ZO-2 was detected in the nucleus of sparse cultures treated for 24 h with the permeable PKCε-activating peptide ψεRACK (Inagaki *et al.*, 2005), confirming (Chamorro *et al.*, 2009) that ZO-2 export from the nucleus is regulated by PKCε phosphorylation.

ZO-2 NLS-1 is functional, whereas NLS-2 is not

Next we analyzed whether the putative bNLSs of ZO-2 are functional. For this purpose we designed a reporter protein nuclear importation assay (Figure 2A, bottom left) in which we microinjected into the cytoplasm of live MDCK cells the reporter protein ovalbumin chemically coupled to a peptide homologous to ZO-2 bNLS-1 or bNLS-2. We coinjected rhodaminated albumin (Rho-alb) as a negative control. After 2 h at 37°C the cells were fixed, permeabilized, and treated with an antibody against ovalbumin and a corresponding secondary antibody coupled to Alexa Fluor 488. The images in Figure 2A (top) and the corresponding quantitative analysis (bottom right) show that bNLS-1-OVA (green) concentrates at the nucleus (blue), whereas bNLS-2-OVA does not appear at the nucleus and instead distributes in the cytoplasm. Rhodaminated albumin (red, top) remains at the microinjection site and is diffusely distributed in the cytoplasm. Taken together, these results indicate that ZO-2 bNLS-1 is functional, whereas bNLS-2 is not.

The arrival of ZO-2 at the nucleus is delayed by phosphomimetic mutations within bNLS-2

On analyzing the sequence of bpNLS-2, we observe that it is a canonical bNLS (Macara, 2001), as it consists of two stretches of basic amino acids separated by a linker region of 10–12 residues

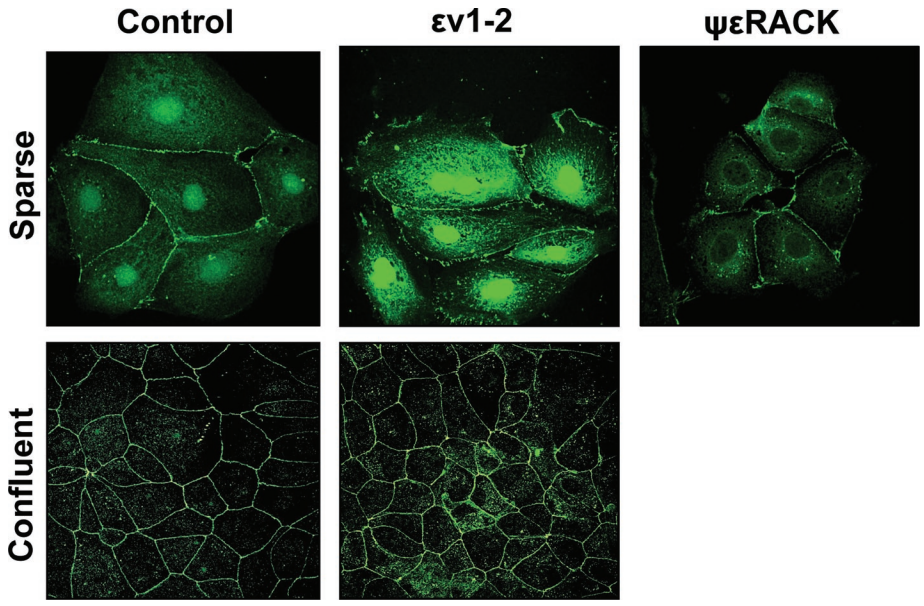

FIGURE 1: In confluent cultures, blocking the nuclear exportation of ZO-2 does not trigger the nuclear accumulation of the protein. MDCK cells were left untreated or incubated for 24 h with 1 μM PKCε permeable inhibitor peptide εv1-2 or PKCε permeable activating peptide ψεRACK. Monolayers were fixed, permeabilized, and processed for immunofluorescence with an antibody against ZO-2 (green). In control sparse cultures ZO-2 is present at the nucleus and cell borders, whereas in control confluent cultures, ZO-2 is absent from the nucleus and concentrates at the cell boundaries. Treatment with εv1-2 conspicuously concentrates ZO-2 at the nucleus of sparse monolayers, whereas no change is observed in confluent cultures. Treatment of sparse monolayers with ψεRACK depletes the nucleus of ZO-2.

(Figure 2A). We noted, however, that it also contains three serine residues (S257, S259, S261) within the carboxyl cluster of three arginine residues, which by in silico analysis constitute putative PKC phosphorylation sites. Therefore we hypothesized that the capacity of bpNLS-2 to import proteins into the nucleus might be hampered by the phosphorylation of these serines, which could neutralize the positive charges present within the NLS. To test this, we next analyzed the intracellular traffic of ZO-2 when serines 257, 259, and 261 were substituted for glutamic acid (S257E, S259E, and S261E) or when S257 was substituted for glutamic acid (S257E) to generate a single phosphomimetic mutation or for alanine (S257A) to eliminate a single phosphorylation site. Figure 3A shows, as we previously reported (Chamorro *et al.*, 2009), that ZO-2 wild type (WT) initially accumulates at the nucleus (time 0 = 6 h after transfection) and departs with time after transfection. Instead, we observe that at time 0, only 24, 41, and 64% of transfected cells, respectively, have the S257E/S259E/S261E, S257E, or S257A mutants at the nucleus, in comparison with the 78% of transfected cells that show ZO-2 WT at the nucleus. Because the nuclear recruitment of ZO-2 is less effective in the triple than in the single phosphomimetic mutant and the S257A mutant exerts a smaller effect than the S257E mutant, we conclude that the phosphorylation of serine residues within bNLS-2 blocks the functionality of the signal and delays nuclear importation of ZO-2. The fact that this blockade is overcome with time after transfection suggests that the additional NLSs within ZO-2, namely bNLS-1 and monopartite NLS, can rescue the nuclear importation of the protein.

Figure 3A also shows that ZO-2 triple and single mutants are still present at the nucleus 24 h after transfection, in contrast to transfected WT ZO-2 (S257E/S259E/S261E, S257E, S257A, and WT have 67, 76, 78, and 17% of cells with nuclear hemagglutinin [HA]–ZO-2 staining, respectively, at 24 h). Because the nuclear recruitment assay gives only a qualitative result indicating the percentage of cells displaying ZO-2 at the nucleus, we next performed a cell fractionation assay and analyzed by Western blot the amount of HA–ZO-2 present in the plasma membrane and nuclear fractions 24 h after ZO-2 transfection. Figure 3B shows that at this time, WT HA–ZO-2 is barely detectable in the nuclear fraction, whereas a considerable amount is present at the plasma membrane. In contrast, S257E HA–ZO-2 mutant accumulates in the nucleus, whereas the S257A mutant is present, albeit in low amounts, at both the nucleus and the plasma membrane. These results indicate that the phosphorylation of S257 blocks the exportation of ZO-2 from the nucleus, whereas the absence of S257 alters but does not completely block the exportation of nuclear ZO-2.

Correct development of three-dimensional cultures requires the presence in ZO-2 of S257, which becomes phosphorylated in mature TJs

Next we analyzed whether ZO-2 phosphorylated at S257 is present in epithelial cells. For this purpose we generated a custom-made antibody against the phosphorylated S257 of ZO-2 (ZO-2 pSer257). The specificity of this antibody was confirmed in a Western blot, which showed a decrease of the p-S257 signal in a cell lysate after phosphatase treatment and in cells transfected with S257A mutant, whereas transfection with wild-type ZO-2 conspicuously increased the staining in comparison to control untransfected cells (Figure 4A).

Then we stained monolayers of MDCK cells at different times after plating with the ZO-2 pSer257 antibody. Figure 4B shows that 12 and 24 h after plating, ZO-2 pSer257 is present at the nuclei. This staining is unspecific, however, as it is also present in confluent ZO-2 knockdown (KD) cells, where no staining for ZO-2 is detected (Figure 4C). Instead, 48 and 72 h after plating, as the monolayers are becoming confluent, ZO-2 pSer257 is found at the cell borders (Figure 4B). These results hence suggest that the phosphorylation of ZO-2 at S257 occurs only in mature TJs. To further test this point, we analyzed the recruitment of ZO-2 pSer257 during new cell–cell contact formation induced by a Ca^{2+} switch. Figure 4D shows how as early as 15 min after the transfer from low-calcium (LC) to normal-calcium (NC) media, ZO-2 is detected at the cellular borders and at 180 min forms a continuous network that encircles all the cells in the culture. Instead, ZO-2 pSer257 starts to appear at 180 min, and at 360 min has not yet formed a continuous "chicken-fence" pattern. In addition, the Western blot in Figure 4E shows that the amount of ZO-2 pSer257 increases with time in a Ca^{2+}-switch assay. Taken together these results indicate that phosphorylation of ZO-2 at S257 is a late event occurring only in mature TJs.

Because one of the canonical functions of TJs is to maintain the polarization of epithelial cells (Mandel *et al.*, 1993) and the absence of ZO-2 is related to alterations in the cytoarchitecture of cell cultures (Hernandez *et al.*, 2007), we next analyzed whether mutations at S257 of ZO-2 could alter the formation of cysts. These

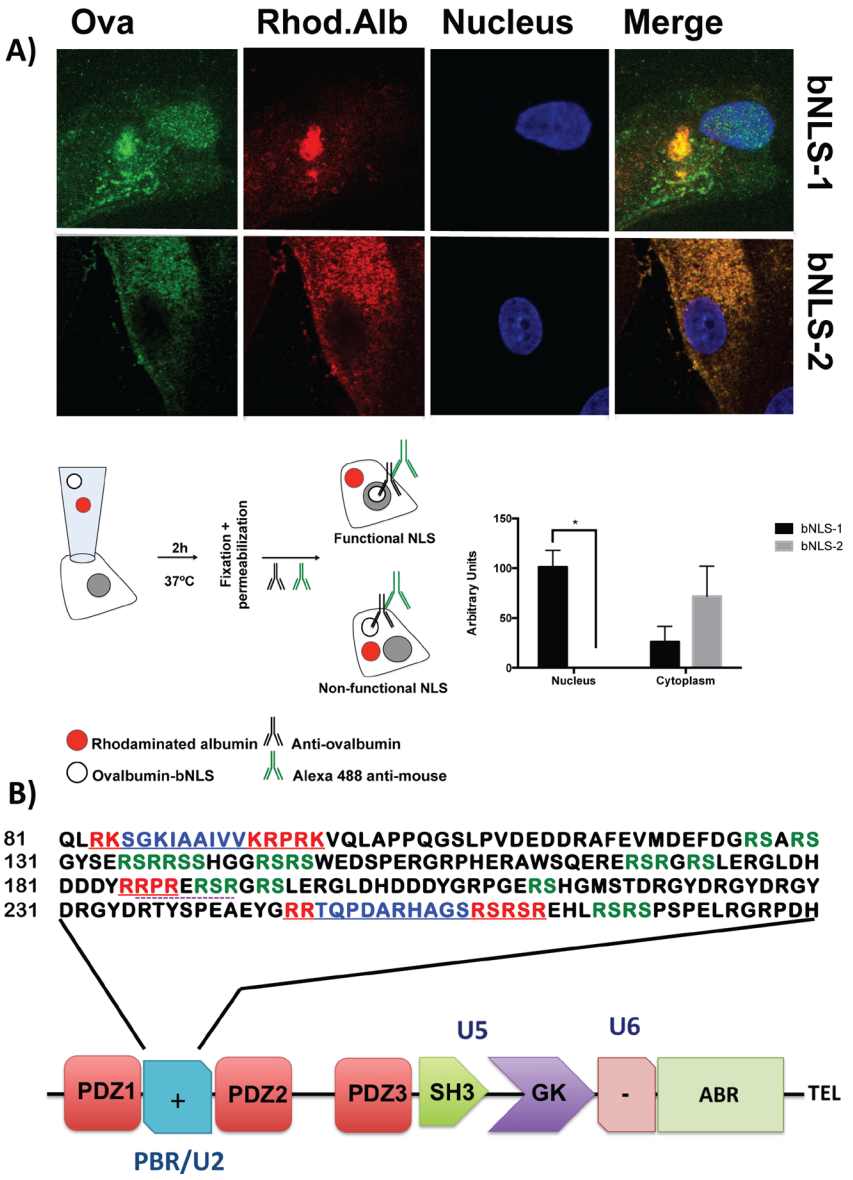

FIGURE 2: ZO-2 sequence has two bNLSs, but only bNLS-1 is functional in a reporter protein nuclear importation assay. (A) Reporter protein nuclear microinjection assay. Bottom, left, schematic representation of the assay, illustrating how the cytoplasm of sparse MDCK cells was microinjected with the reporter protein ovalbumin chemically coupled to a peptide homologous to ZO-2 bNLSs (bNLS-1-OVA or bNLS-2-OVA) and rhodaminated albumin (Rho-Alb). After a 2-h incubation at 37°C, the cells were fixed and processed for immunofluorescence with an antibody against ovalbumin and a corresponding secondary antibody coupled to Alexa Fluor 488. Top, immunofluorescence obtained from the nuclear importation assay. Bottom right, quantitative analysis of ovalbumin fluorescence signal intensity in the nucleus and cytoplasm made with ImageJ (National Institutes of Health, Bethesda, MD) particle analysis. Results from three independent experiments. *$p < 0.05$ as assessed by two-way analysis of variance (ANOVA) followed by Bonferroni's post hoc test. bNLS-1-OVA (green) concentrates at the nucleus stained in blue with TO-PRO-3 (blue), whereas rhodaminated albumin (red) distributes in the cytoplasm. bNLS-2-OVA does not travel to the nucleus and remains in the cytoplasm. (B) Schematic representation of ZO-2 showing a polybasic region (+) located at the amino-terminal segment of PDZ-1 and the beginning of the U2 linker between PDZ-1 and PDZ-2 domains. This region contains 16 RS motifs (green), three NLSs (underlined), and a SRPK1-binding motif (dotted line). The clusters of basic K and/or R amino acids in the NLS are shown in red, and the spacer amino acids within the two bNLSs are marked in blue.

three-dimensional (3D) cultures, obtained by growing cells in the extracellular matrix Matrigel, recapitulate several features of epithelial tissues in vivo and therefore provide an ideal model in which to study epithelial morphogenesis and polarity under more physiological conditions (Elia and Lippincott-Schwartz, 2009). Figure 5 shows that cysts formed with cells transiently transfected with wild-type HA–ZO-2 are typical and as previously reported (Elia and Lippincott-Schwartz, 2009) have a hollow lumen surrounded by one layer of polarized cells, where the apical surface facing the lumen is stained with gp135/podocalyxin, whereas those formed with cells transfected with S257A or S257E HA–ZO-2 mutants display multiple lumens. In the cysts, HA–ZO-2 (green staining) is present throughout the cytoplasm, as expected for a transfected cell where the protein is overexpressed, but is absent from the nucleus. This was foreseeable since the cysts are 8 d old and, as shown in Figure 1, ZO-2 makes no detour to the nucleus in confluent cultures.

In summary, these results suggest that the presence of S257 in ZO-2 is required for the correct epithelial morphogenesis to develop and that as the TJ matures, ZO-2 becomes phosphorylated at S257.

aPKCζ phosphorylates ZO-2 at S257

Our next aim was to identify the kinase that phosphorylates ZO-2 at S257. According to the in silico analysis S257 is a putative phosphorylation site for PKC. Therefore we treated confluent cultures of MDCK for 24 h with the broad-spectrum PKC inhibitor Gö 6850 (Song *et al.*, 2001). Figure 6 shows that the cell-border staining of ZO-2 pSer257 is lost after treatment with 6 μM Gö 6850, suggesting that the phosphorylation of ZO-2 at S257 is due to PKC. To further determine the PKC isozyme involved, we next incubated the monolayers with 2 μM Gö 6850, since at this concentration PKC α, β, γ, δ, and ε isoforms are inhibited but aPKCζ is not. Figure 6 shows that with 2 μM Gö 6850 the cell-border pattern of ZO-2 S257-P is maintained, suggesting that PKC ζ might be the PKC isozyme responsible for S257 phosphorylation. To support this observation, we next treated the monolayers with a specific PKCζ inhibitor, the myristoylated permeable PKCζ pseudosubstrate (Standaert *et al.*, 1997), and observed that ZO-2 pSer257 is no longer present at the cell borders. Of interest, the cell-border staining obtained with the anti–ZO-2 antibody diminishes but does not disappear in the monolayers treated with PKCζ pseudosubstrate, suggesting that although a considerable amount of ZO-2 is phosphorylated at S257 in mature TJs, another pool of ZO-2 not S257 phosphorylated is also present.

Taken together these results indicate that PKCζ is responsible for the phosphorylation of ZO-2 at S257 in mature TJs.

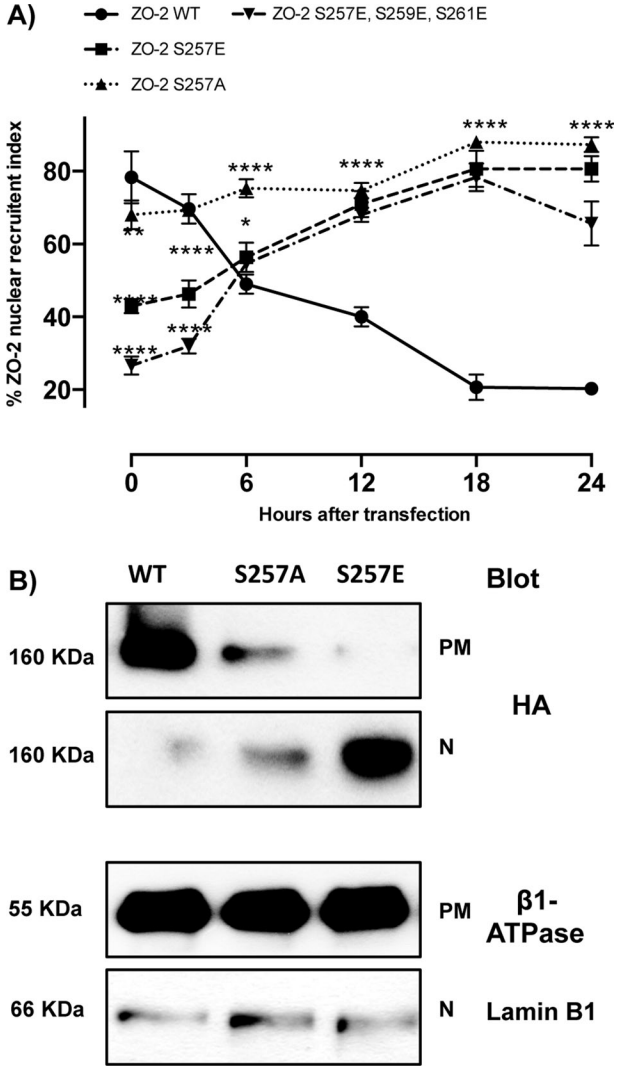

FIGURE 3: ZO-2 triple mutant S257E/S259E/S261E and the single mutants S257E and S257A arrive at the nucleus with a delay. (A) Percentage of cells with nuclear HA–ZO-2 as a function of time. The percentage of cells with nuclear ZO-2 was determined by immunofluorescence using an anti-HA antibody. Monolayers were fixed at the indicated times. Time 0 corresponds to 6 h after transfection. Experiments were done with cells transfected with full-length HA–ZO-2 (WT), the triple mutant S257E/S259E/S261E and single mutants S257E and S257A. Results from three independent experiments. In each experiment 100 transfected cells were evaluated per experimental point. *$p < 0.05$, **$p < 0.01$, ***$p < 0.001$, and ****$p < 0.0001$ with respect to ZO-2 WT as assessed by two-way ANOVA followed by Bonferroni's post hoc test. (B) Detection by Western blot of HA–ZO-2 present in plasma membrane and nuclear fractions derived from cells 24 h after being transfected with HA–ZO-2 WT or the mutants S257A and S257E. Lamin B1 and Na^+-K^+-ATPase β1 subunit antibodies were used as positive controls of nuclear and plasma membrane fractions, respectively.

The *O*-linked β-*N*-acetylglucosamination of ZO-2 at S257 promotes the nuclear exportation of the protein

Figure 3A shows that although newly synthesized ZO-2 mutant S257A arrives at the nucleus in a manner similar to wild-type ZO-2, it cannot depart from the nucleus, as no decrease in the nuclear recruitment index is observed with time after transfection. This result suggests that S257 plays a critical role in the nuclear exportation of ZO-2.

In silico analysis (YinOYang 1.2; www.cbs.dtu.dk/services/YinOYang/) shows that S257 is a Yin-Yang site, meaning that there might be competitive and alternative occupancy of this residue as it constitutes an attachment site for both an *O*-phosphate and an *O*-GlcNAc (Hart *et al.*, 2007). Therefore we next analyzed whether ZO-2 is *O*-GlcNAcylated and the effect of this modification on the subcellular localization of the protein. Figure 7A shows that endogenous or transfected ZO-2 immunoprecipitated respectively with an antibody against ZO-2 or the tag HA gives a strong positive reaction when blotted with an antibody against *O*-GlcNAc. We then immunoprecipitated endogenous ZO-2 from MDCK cell nuclear or membrane fractions and observed with the antibody against *O*-GlcNAc a positive reaction only when ZO-2 is derived from the nuclear fraction (Figure 7B). This result hence indicates that ZO-2 is being *O*-GlcNAcylated at the nucleus.

To further identify the region of ZO-2 being *O*-GlcNAcylated, we next transfected MDCK cells with two constructs corresponding to different segments of ZO-2: amino (three PDZ domains: amino acids [aa] 1–588) and AP (acidic and proline-rich domains: aa 878–1170). Because ZO-2 *O*-GlcNAcylation takes place at the nucleus, we excluded the 3PSG construct (PDZ-3, SH3, and GUK domains: aa 402–874) because we previously showed that this ZO-2 segment does not travel to the nucleus (Jaramillo *et al.*, 2004). Figure 7C shows that when the amino and AP segments were purified from an MDCK cell extract with an affinity Tag column and blotted with an antibody against *O*-GlcNAc, only the amino segment showed *O*-GlcNAcylation. Next we tested whether mutation S257A ablated the *O*-GlcNAcylation of the amino segment. For this purpose we transfected MDCK cells with ZO-2 amino WT and amino S257A, immunoprecipitated with an anti ZO-2 antibody and blotted against *O*-GlcNAc. Figure 7D (left) shows that the *O*-GlcNAcylation signal is lost in the S257A ZO-2 amino mutant segment present as a 75-kDa band when blotted with the antibody against the Xpress tag. When the same experiment was done transfecting full-length ZO-2 WT or the mutant S257A we observed a very small decrease in the *O*-GlcNAcylation signal (Figure 7D, right), indicating that additional *O*-GlcNAcylation sites might be present in ZO-2 outside of the amino segment and probably at the 3PSG segment. In summary, these results indicate that ZO-2 is an *O*-GlcNAcylated protein and that one of the places where this modification takes place is at S257.

Stabilizing the *O*-GlcNAcylation of ZO-2 promotes the degradation of the protein

To test the impact of *O*-GlcNAcylation in the stability and subcellular localization of ZO-2, we used *O*-(2-acetamido-2-deoxy-D-glucopyranosylidene)amino-*N*-phenylcarbamate (PUGNAc), which is a GlcNAc analogue that inhibits *O*-GlcNAc hydrolase, the enzyme that removes *O*-GlcNAc from proteins (Haltiwanger *et al.*, 1998). Treatment with PUGNAc inhibits *O*-GlcNAc turnover and increases *O*-GlcNAcylation levels of a variety of proteins (Haltiwanger *et al.*, 1998).

Figure 8A (left) shows by Western blot that treatment for 16 h with PUGNAc produces an increase in the *O*-GlcNAcylation of cell extracts. By immunofluorescence we observe that under this same treatment, the nuclei become depleted of ZO-2 (top right, middle), and quantitative analysis of ZO-2 fluorescence signal intensity shows a significant decrease in the nuclear staining of ZO-2 in PUGNAc-treated cells (bottom right), suggesting that *O*-GlcNAcylation prompts the nuclear exportation of ZO-2. Figure 8A (top right, middle) also shows loss of ZO-2 staining at some cell borders, suggesting decreased stability of ZO-2 on increasing *O*-GlcNAcylation, as has been shown for other proteins treated with PUGNAc (Srikanth

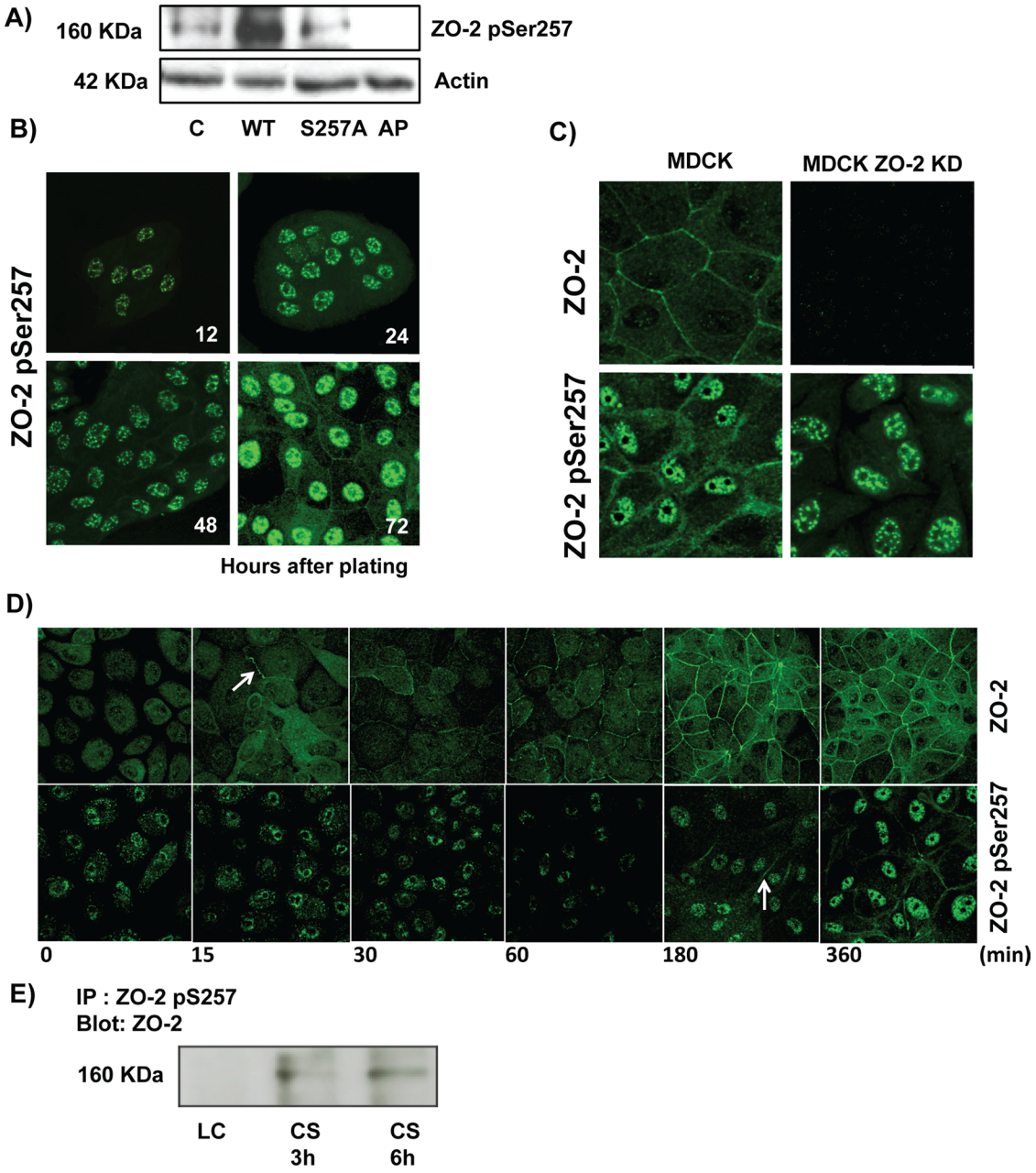

FIGURE 4: Phosphorylation of ZO-2 at S257 occurs in mature TJs. (A) Western blot with the antibody against ZO-2 S257-P in a lysate derived from control cells (C) untreated or after alkaline phosphatase treatment (AP) or in cells transfected with WT ZO-2 or ZO-2 mutant S257A. (B) ZO-2 S257-P is present at the cell borders at late but not at early times after plating. MDCK monolayers plated at subconfluent density were fixed at different times after plating and processed for immunofluorescence with a specific antibody against ZO-2 S257-P. (C) Nuclear staining with the antibody against ZO-2 S257-P is unspecific. An antibody against ZO-2 gives no staining in ZO-2 KD monolayers, whereas the ZO-2 S257-P antibody gives a nuclear labeling in ZO-2-KD cells. (D) Phosphorylation of ZO-2 at S257 occurs in mature TJs. ZO-2 appears at the cell borders 15 min after the Ca^{2+} switch, whereas ZO-2 S257-P is detected 180 min after transfer to NC. (E) The amount of ZO-2 S257-P increases as cell–cell contacts mature in a Ca^{2+} switch assay. ZO-2 S257-P was immunoprecipitated from monolayers incubated 20 h in low calcium or subsequently transferred to normal calcium for 3 and 6 h.

et al., 2010). To test this point, we coincubated the cells for 16 h with both PUGNAc and the proteosomal inhibitor MG132 (Lee and Goldberg, 1998). Figure 8A, right, shows increased and diffuse expression of ZO-2 in the cytoplasm and the absence of ZO-2 from the nuclei, and quantitative analysis of ZO-2 fluorescence signal intensity confirms a significant decrease in nuclear staining and an increase in cytoplasmic ZO-2 in cells treated with PUGNAc and MG132 in comparison to untreated cells (bottom right). Western blot analysis of ZO-2 in nuclear, cytoplasm and plasma membrane fractions (Figure 8B, left) and the corresponding densitometric analysis of ZO-2 signal (Figure 8B, right) showed that after 16 h of treatment with PUGNAc the amount of ZO-2 present at the nucleus and

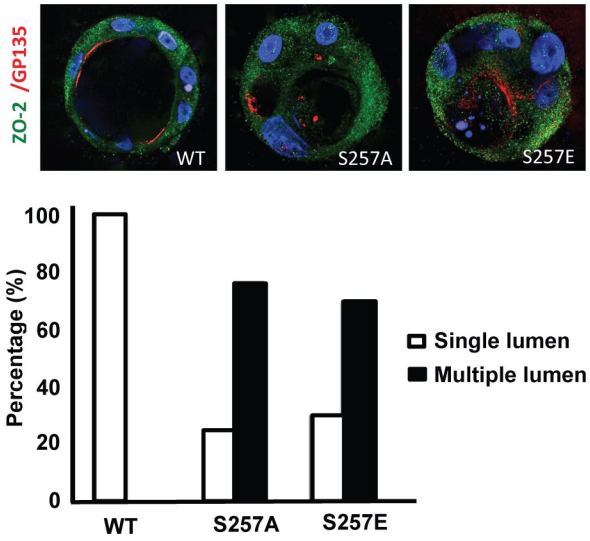

FIGURE 5: S257 in ZO-2 is required for the correct formation of cysts. MDCK cells transfected with ZO-2 WT or the mutant S257A or S257E were incubated with Matrigel and observed 8 d later to allow the formation of cell cysts. Cysts were fixed and processed for immunofluorescence with antibodies against ZO-2 (green) and gp135/podocalyxin (red). The nuclei were stained in blue with DAPI dissolved in mounting medium. The images (top) and the graph with the quantitated data (bottom) show that the substitution of S257 with either alanine or glutamic acid induces the aberrant formation of multiple lumens per cyst. A total of 50 cysts were analyzed per experimental condition. In comparison to WT all conditions were statistically significant, $p < 0.001$, using a chi-squared test.

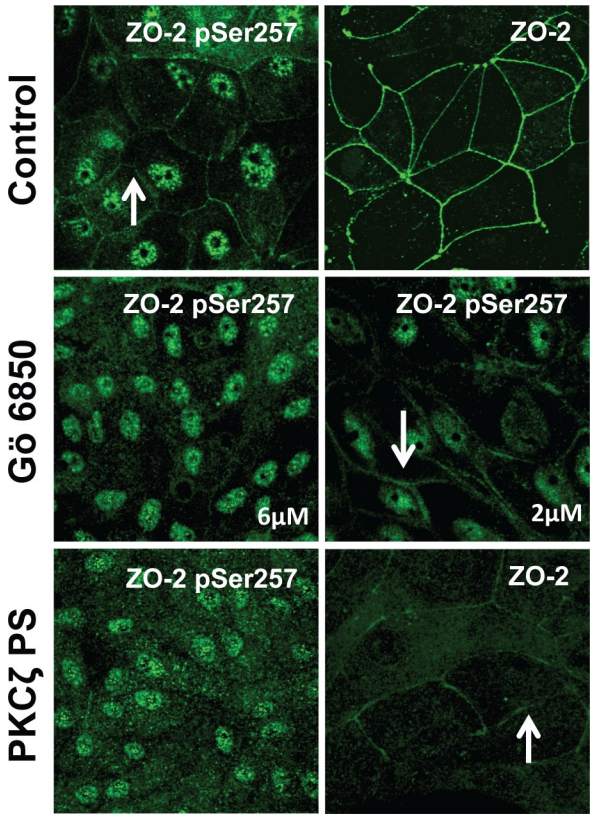

Gö 6805

- **6 μM (α, β, γ, δ, ε, and ζ)**
- **2 μM (α, β, γ, δ and ε)**

FIGURE 6: PKCζ phosphorylates ZO-2 at S257. MDCK cells were plated at confluence density in the absence or presence of 2 or 6 μM Gö 6850 or 10 μM PKCζ pseudosubstrate. One day later the monolayers were fixed and processed for immunofluorescence with antibodies against ZO-2 or ZO-2 S257-P. Observe the disappearance of the "chicken-fence" pattern of ZO-2 S257-P upon treatment with PKCζ pseudosubstrate (PS) or 6 μM Gö 6850.

plasma membrane fractions diminishes significantly and that treatment with PUGNAc plus MG132 allows the detection of ZO-2 at the plasma membrane but not at the nucleus. Taken together, these results confirm that *O*-GlcNAcylation of ZO-2 promotes the nuclear exportation of the protein and indicate that if ZO-2 remains *O*-GlcNAcylated, it is no longer directed to the TJs and phosphorylated at S257 and instead becomes degraded at the proteosome.

To further explore the degradation of *O*-GlcNAcylated ZO-2, we used the in situ proximity ligation assay Duolink. This assay allowed us to use one antibody to detect ZO-2 and another antibody to *O*-GlcNAcylation, so that a signal visible as discrete fluorescent spots would be generated when the two antibodies were bound in proximity closer to 40 nm. Figure 8C shows that in control condition positive fluorescent spots are present at the nucleus and cytoplasm but not at the cell borders (left) and that treatment for 16 h with PUGNAc completely obliterates the signal (middle), which is partially restored by incubation with the protease inhibitor MG132 (right). These results confirm that *O*-GlcNAcylated ZO-2 is present at the nucleus and cytoplasm but not at the TJ region and that stabilization of *O*-GlcNAc by PUGNAc induces degradation of ZO-2.

Phosphorylation of SR motifs in ZO-2 by SRPK1 induces the transport of the protein to the nucleus

SR proteins are splicing factors characterized by the presence of an RNA recognition motif (RRM) and SR dipeptides. Because we previously observed in the sequence of cZO-2 the presence of 16 SR motifs (Jaramillo *et al.*, 2004; Figure 2B), we next searched for RRMs but did not find the consensus sequence 1 (Adam *et al.*, 1986) or 2 (Dreyfuss *et al.*, 1988). Using BindN (bioinfo.ggc.org/bindn), however, a Web-based tool for the prediction of RNA-binding sites, we found, with 98% sensitivity, seven binding sites: aa 129–147, 187–192, 257–274, 676–685, 815–821, 981–*985, and 1160–1168.

SR proteins are extensively phosphorylated at their SR motifs by SRPKs. The latter constitute a subfamily of serine-threonine kinases that specifically phosphorylate serine residues residing in serine-arginine/arginine-serine dipeptide motifs (for review see Giannakouros *et al.*, 2011). Phosphorylation by SRPK1, the isoform with a broader tissue distribution, requires in its substrates the presence of a docking motif with the consensus sequence RXR/KXXXR (where X is any amino acid; Ngo *et al.*, 2005). In cZO-2 we observe, within the U2 linker (aa 186–192), the presence of an SRPK1 docking motif (Figure 2B), and therefore we next analyzed whether ZO-2 and SRPK1 are associated. For this purpose we transfected MDCK cells with an hSRPK1-FLAG construct or the empty vector pCMV and performed a Duolink assay with one antibody against ZO-2 and another against FLAG. Figure 9A shows positive fluorescent spots in the cytoplasm but not the nucleus of cells transfected with SRPK1, suggesting that ZO-2 is associated with SRPK1 in the cytoplasm.

Next we analyzed whether the transfection with SRPK1 increased the phosphorylation of ZO-2. For this purpose we transfected MDCK cells with HA–ZO-2 and SRPK1-FLAG and observed that the

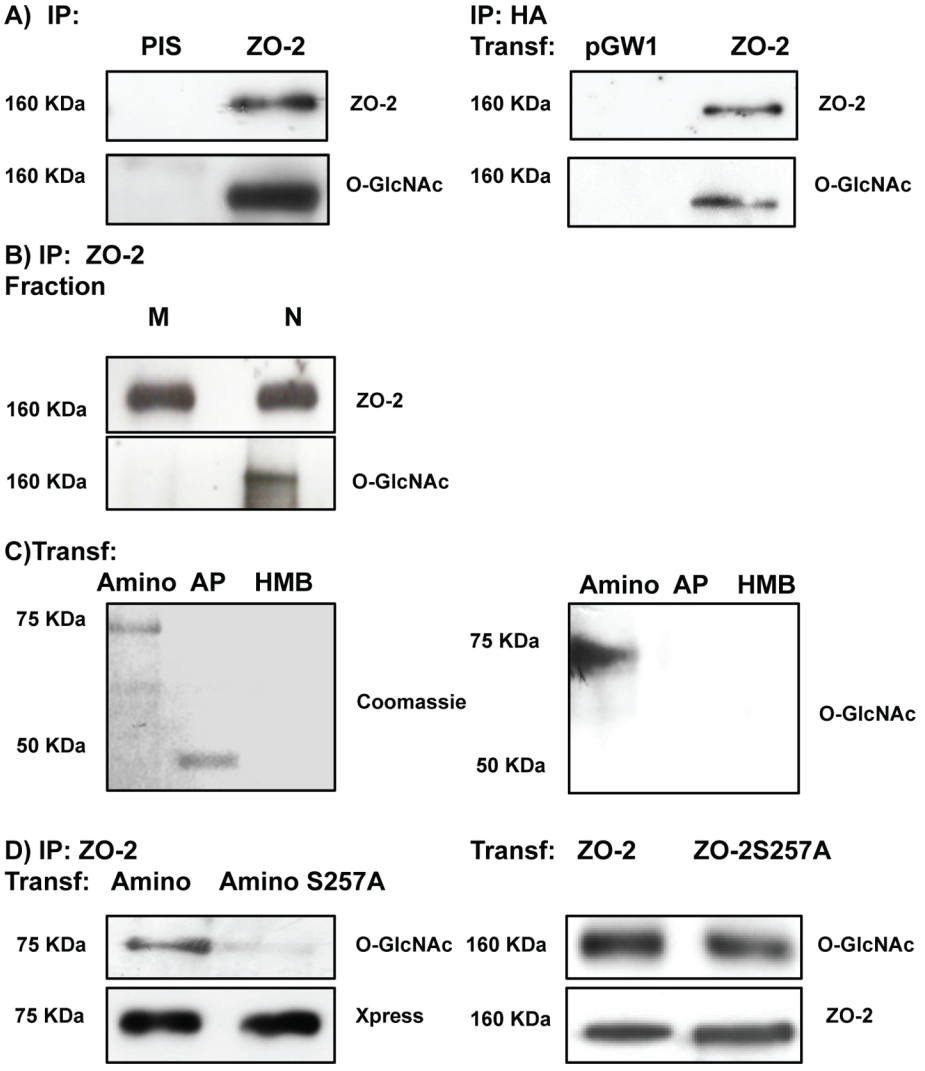

FIGURE 7: ZO-2 is *O*-GlcNAcylated at the nucleus at S257. (A) ZO-2 is an *O*-GlcNAcylated protein. Endogenous (left) or exogenous (right) ZO-2 was immunoprecipitated with antibodies against ZO-2 (left) or HA (right) and blotted with antibodies against ZO-2, HA, or *O*-GlcNAc. PIS, preimmune serum; pGW1, empty vector. (B) *O*-GlcNAcylated ZO-2 is present in the nucleus but not in the plasma membrane. Endogenous ZO-2 was immunoprecipitated from a membrane (M) or nuclear (N) fraction derived from MDCK cells and blotted with an antibody against *O*-GlcNAc. (C) The amino and not the AP segment of ZO-2 is *O*-GlcNAcylated. MDCK cells were transfected with amino and AP histidine-tagged constructs of ZO-2. The corresponding proteins were purified by Ni affinity columns, run in SDS–PAGE, stained with Coomassie blue, and blotted with an antibody against *O*-GlcNAc. HMB, empty vector HisMax B. (D) ZO-2 is *O*-GlcNAcylated at S257 and elsewhere outside of the amino segment. MDCK cells were transfected with ZO-2 WT amino or amino 257A constructs (left) or ZO-2 full-length WT or mutant 257A (right). ZO-2 was immunoprecipitated, run on SDS–PAGE, and blotted against *O*-GlcNAc and the Xpress tag. Transf, transfection.

immunoprecipitated HA–ZO-2 displayed a higher amount of phosphorylated serine residues than cells nontransfected with SRPK1-FLAG (Figure 9B, top left). To further test this, we performed pSer/ZO-2 densitometric analysis of the upper– and lower–molecular weight bands of ZO-2, which showed a significant increase in pSer/ZO-2 in cells transfected with SRPK1 (Figure 9B, bottom). To additionally confirm this point, we performed a mobility shift detection assay of ZO-2. For this, we run extracts of MDCK cells transfected with HA–ZO-2 or HA–ZO-2 and SRPK1-FLAG on phosphate-affinity SDS–PAGE with a dinuclear manganese complex of acrylamide-pendant Phos-tag, which selectively binds and retards the migration of phosphorylated proteins. Figure 9B (right) shows that the transfection of SRPK1-FLAG induces slower migration of the ZO-2 band in comparison to its characteristic one (160 kDa) present in cells nontransfected with SRPK1. This result indicates that overexpression of SRPK1 induces hyperphosphorylation of ZO-2.

Then we analyzed the effect of SR repeat phosphorylation by SRPK1 on the localization of ZO-2. Figure 9C (first column) shows that in sparse cultures transfected with SRPK1, ZO-2 concentrates in the nucleus (arrow) and disappears from the cell borders (arrowhead), whereas none of these effects is detected in untransfected cells (asterisk) or in cells transfected with the empty vector (second column). In confluent cultures we observe that the transfection of SRPK1 induces a strong expression of ZO-2 in the cytoplasm but not its concentration in the nucleus (third column). These results suggest that phosphorylation of SR residues induced by overexpression of SRPK1 triggers movement of ZO-2 into the nucleus in sparse but not in confluent cultures.

Previously we demonstrated that ZO-2 overexpression inhibits the cell proliferation rate of sparse epithelial cells (Huerta *et al.*, 2007; Tapia *et al.*, 2009). Therefore we next explored whether in sparse cultures, nuclear ZO-2 acted as an inhibitor of proliferation. For this purpose we transfected sparse MDCK cells with SRPK1 to induce the nuclear accumulation of ZO-2. Supplemental Figure S1 shows a decreased cell proliferation rate in SRPK1-transfected cells in comparison to cells transfected with the empty vector, suggesting that nuclear ZO-2 reduces cells proliferation. Because we recently identified a novel ZO-2–associated protein named ZASP whose overexpression blocks the inhibitory activity of ZO-2 on cyclin D1 (CD1) gene transcription and protein expression (Lechuga *et al.*, 2010), we next tested whether SRPK1 transfection could alter the nuclear distribution of ZASP. Supplemental Figure S2 shows that in cells transfected with SRPK1, ZASP is displaced from the nuclei and accumulates at the cytoplasm. This result suggests that the nuclear accumulation of ZO-2 triggered by SRPK1 overexpression has the functional consequence of promoting the exit from the nucleus of a factor that promotes the expression of CD1.

Activation of SRPK1 induced by EGF through Akt induces serine phosphorylation of ZO-2 and triggers speckled nuclear distribution of the protein

We next analyzed whether activation of SRPK1 could induce nuclear accumulation of ZO-2 in speckles. Recently it was shown that SRPK1 is autophosphorylated and activated in response to EGF signaling through Akt (Zhou *et al.*, 2012). Therefore we

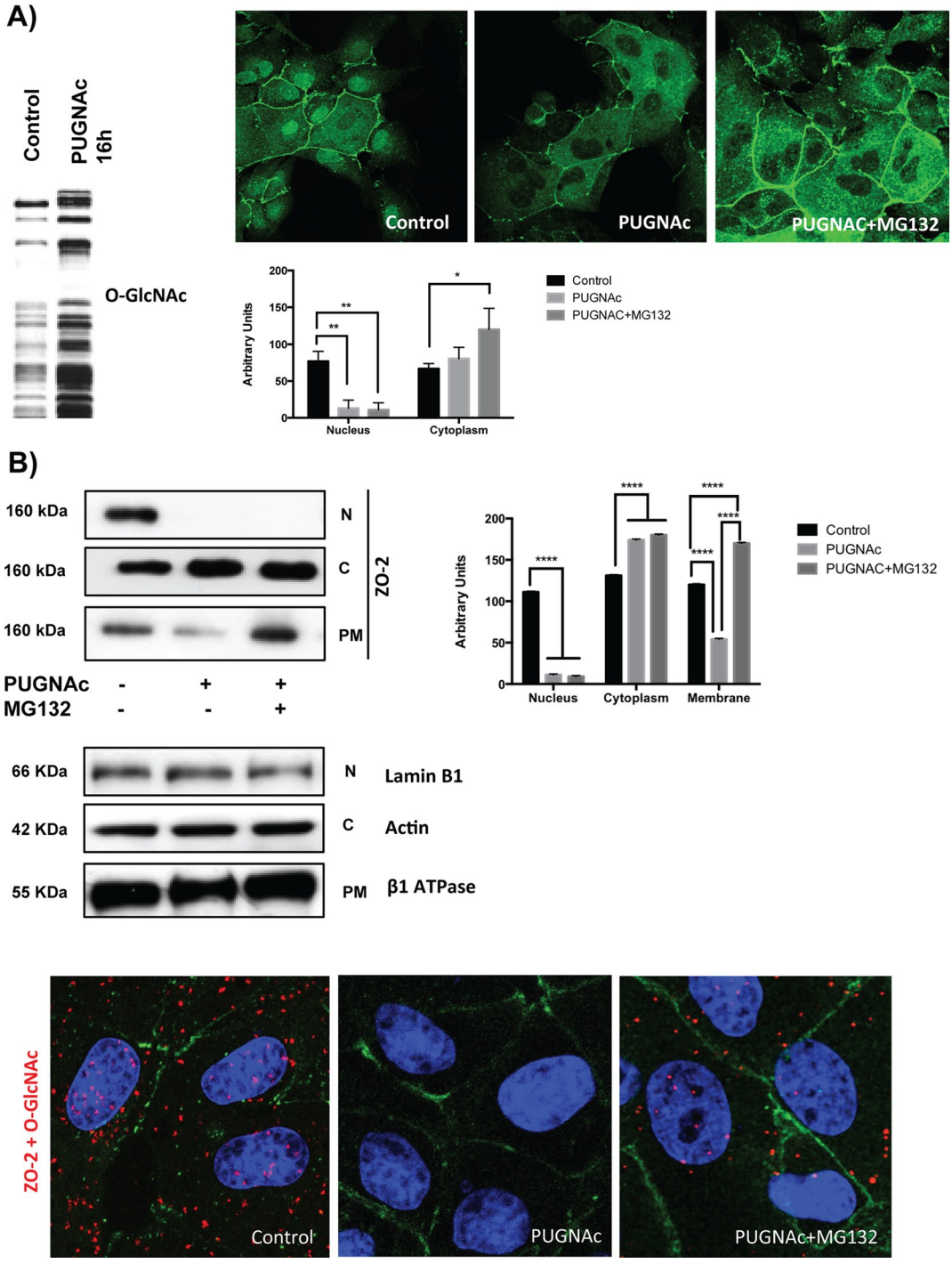

FIGURE 8: PUGNAc-induced stabilization of *O*-GlcNAcylation promotes nuclear exportation and degradation of ZO-2. Sparse cultures of MDCK cells were treated or not for 16 h with 100 µM PUGNAc or 100 µM PUGNAc plus 30 mM MG132. (A) Western blot detection of *O*-GlcNAc in MDCK cell extracts treated or not with PUGNAc (left). PUGNAc induces the disappearance of ZO-2 from the nuclei and cellular borders. Monolayers were fixed and processed for immunofluorescence with an antibody against ZO-2. The quantitative analysis of ZO-2 fluorescence signal intensity in the nucleus and cytoplasm was made with ImageJ particle analysis (bottom right). Results from three independent experiments. $*p < 0.05$ and $**p < 0.01$ as assessed by two-way ANOVA followed by Bonferroni's post hoc test. (B) Treatment with PUGNAc decreases nuclear ZO-2. Left, Western blot against ZO-2 of nuclear (N), cytoplasmic (C), and plasma membrane (PM) fractions derived from cells treated or not with PUGNAc or PUGNAc plus MG132. Antibodies against β_1-Na^+-K^+-ATPase, actin, and lamin B1 were used as positive controls of PM, C, and N fractions, respectively. Right, densitometric analysis of the Western blot. Results from three independent experiments. $*p < 0.05$, $**p < 0.01$, and $****p < 0.0001$ as assessed by two-way ANOVA followed by Bonferroni's post hoc test. (C) Treatment with PUGNAc ablates the expression of *O*-GlcNAcylated ZO-2. The Duolink in situ immunoassay was done with an antibody against ZO-2 and another antibody against *O*-GlcNAc. Cell borders and nuclei were respectively stained with anti–E-cadherin antibody and DAPI.

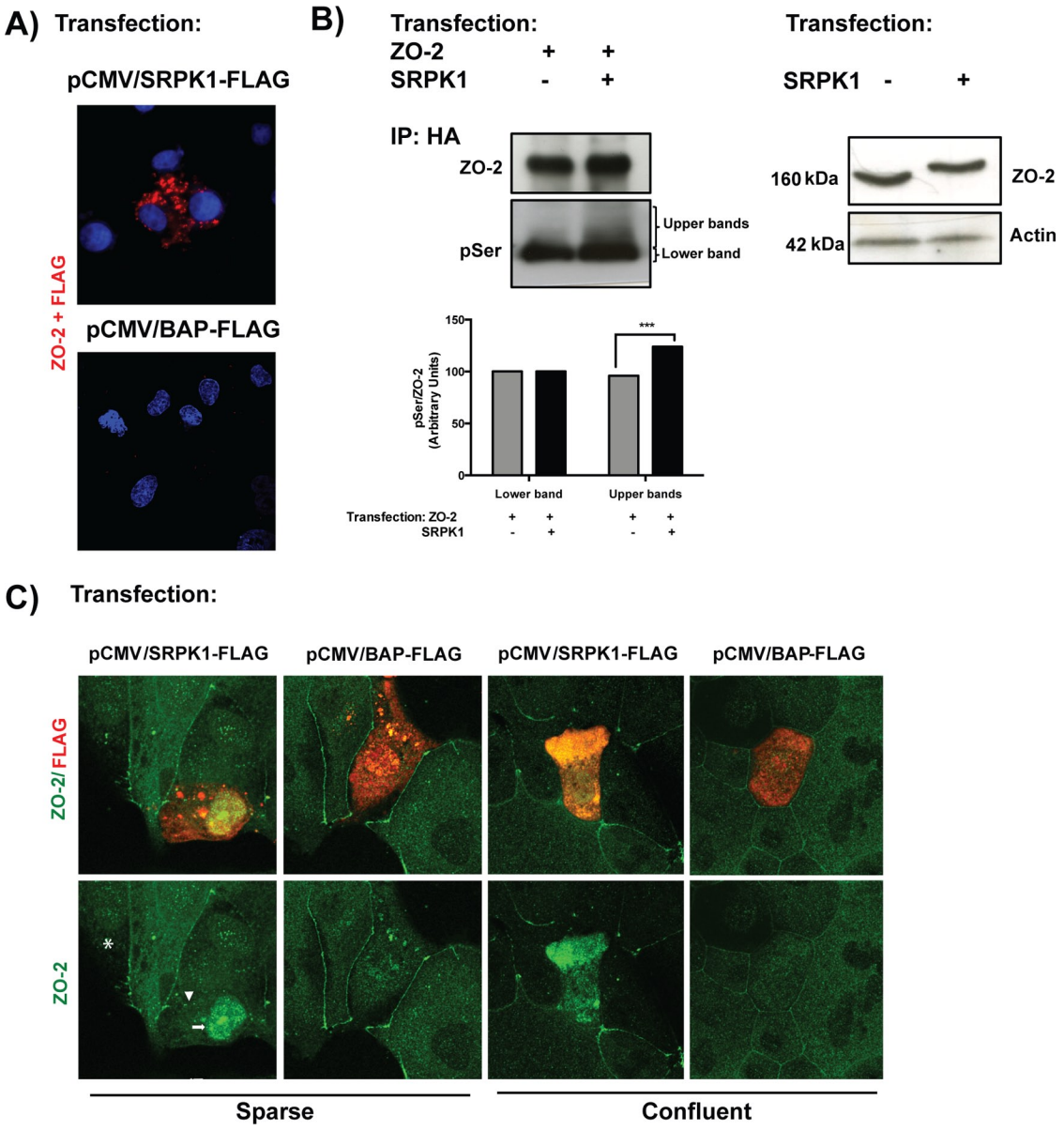

FIGURE 9: SRPK1 phosphorylation of ZO-2 SR motifs induces the transport of the protein to the nucleus. (A) ZO-2 and SRPK1 associate in the cytoplasm. Duolink assay done with antibodies against ZO-2 and against FLAG in MDCK cells transfected with SRPK1-FLAG or the empty vector pCMV. Nuclei were stained in blue with DAPI. (B) Overexpression of SRPK1 induces serine hyperphosphorylation of ZO-2. Top left, MDCK cells were transfected with HA–ZO-2 or HA–ZO-2 plus SRPK1. Exogenous ZO-2 was immunoprecipitated with an anti-HA antibody and blotted with anti-pSer antibody, stripped, and blotted with anti–ZO-2. Bottom, densitometric analysis of the pSer/ZO-2 signal present in the upper and lower bands of the top left blot. In comparison to ZO-2 WT, ZO-2 WT/SRPK1 cotransfection was statistically significant, $p < 0.001$, using a chi-squared test. Top right, a total cellular extract of MDCK cells was transfected or not with SRPK1 and run on an SDS–PAGE with acrylamide-pendant Phos-tag. (C) Overexpression of SRPK1 induces the transport of ZO-2 into the nucleus. In sparse cells transfected with SRPK1, ZO-2 concentrates at the nucleus (arrow) and disappears from the cell borders (arrowhead).

analyzed whether EGF signaling through Akt induced the speckled appearance of ZO-2 at the nucleus. Figure 10A (top) shows that treatment with 100 nM EGF for 24 h induces the appearance of ZO-2 in nuclear speckles and that this process is mediated by Akt, since treatment for 24 h with 30 nM of triciribine (TCN), a selective inhibitor of Akt (Yang *et al.*, 2004), blocks the EGF effect. To demonstrate the participation of SRPK1 in this process, we transfected the cells with a small interfering RNA (siRNA) capable of decreasing SRPK1 protein expression (Figure 10C) and observed that EGF could no longer induce the nuclear accumulation of ZO-2 in speckles.

Next we tested whether SRPK1 activation through EGF signaling incremented the level of ZO-2 serine phosphorylation. For this purpose we performed a Duolink assay with one antibody against ZO-2 and another against pSer. Figure 10A (bottom) shows that upon treatment with EGF, positive fluorescent spots become abundant in the cytoplasm and the nucleus in comparison to control cells, indicating that EGF induces the hyperphosphorylation of ZO-2 at serine

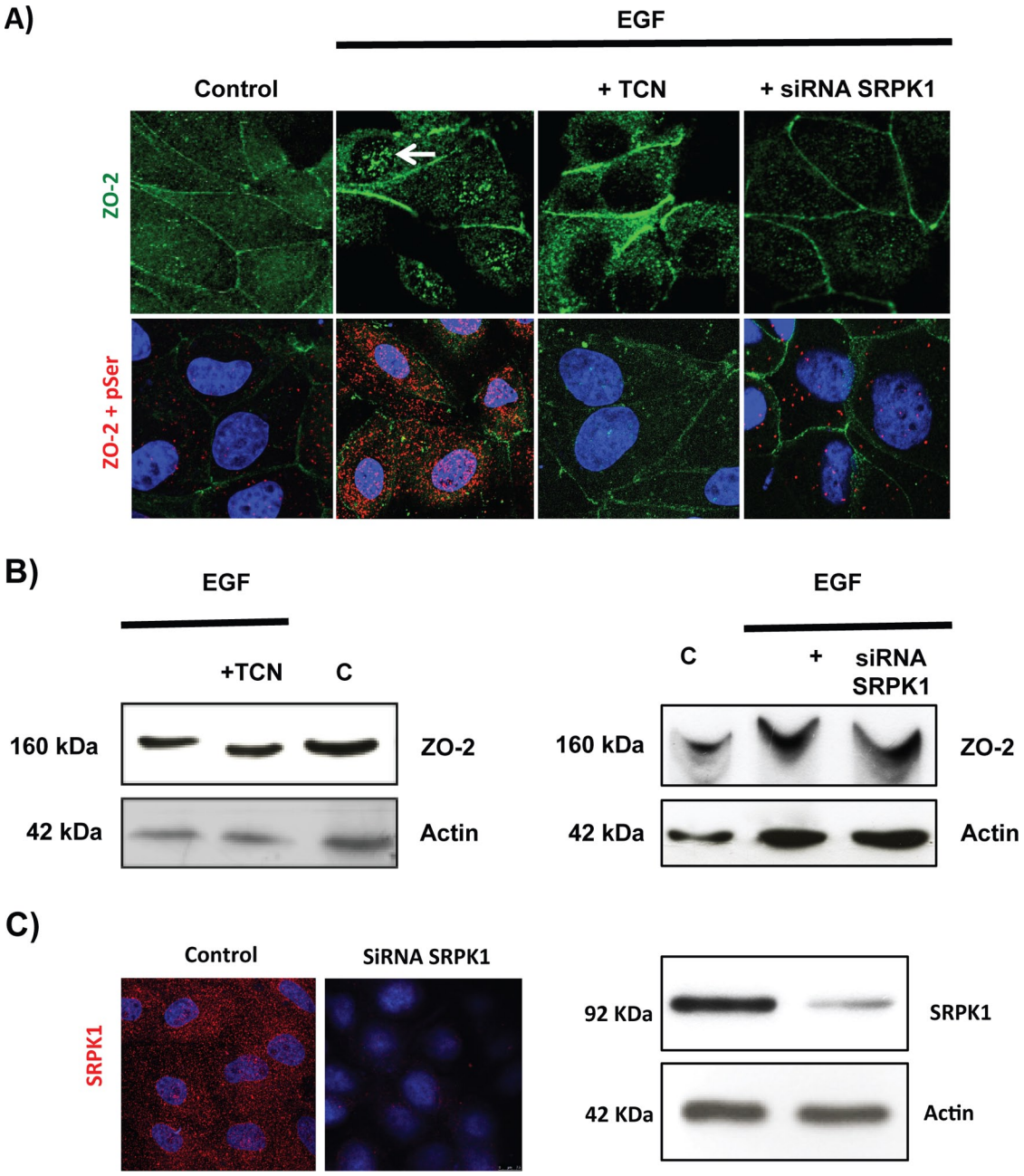

FIGURE 10: EGF induces, via Akt and with the participation of SRPK1, phosphorylation of ZO-2 in serine residues and triggers accumulation of the protein in nuclear speckles. Sparse cultures of MDCK cells transfected or not with a siRNA for SRPK1 were treated for 24 h with 100 nM EGF or EGF plus 30 nM TCN. (A) Top, treatment with EGF induces the appearance of ZO-2 in nuclear speckles (arrow) through a process sensitive to AKT inhibition with TCN and mediated by the presence of SRPK1. Cells were fixed and processed for immunofluorescence with antibodies against ZO-2. Bottom, EGF triggers increased phosphorylation of ZO-2 at serine residues through a process mediated by Akt and requiring the expression of SRPK1. The Duolink in situ immunoassay was done with an antibody against ZO-2 and an antibody against pSer. Cell borders were stained with an anti–E-cadherin antibody. (B) The shift in the ZO-2 band triggered by EGF in an SDS–PAGE with acrylamide-pendant Phos-tag disappeared upon incubation with TCN or by transfection of MDCK cells with a siRNA for SRPK1. (C) Transfection of a siRNA for SRPK1 decreases in MDCK cells the immunofluorescence (left, red) and Western blot (right) signals of the protein detected with a specific antibody against SRPK1. Nuclei were stained with DAPI.

residues. Most of these positive spots are lost upon addition of TCN or a siRNA against SRPK1. Taken together these results indicate that the enhanced phosphorylation in serine residues of ZO-2 triggered by EGF is mediated by the AKT-SRPK1-SR axis.

To further demonstrate the EGF induced phosphorylation of ZO-2, we next analyzed on a phosphate-affinity SDS–PAGE with Phos-tag whether treatment with EGF retarded the band of ZO-2. Figure 10B shows a ZO-2 band shift induced by EGF and blocked

by TCN or a siRNA for SRPK1, confirming that activation of the AKT-SRPK1-SR route induced by EGF produces hyperphosphorylation of ZO-2.

DISCUSSION

Here we studied the intracellular traffic of ZO-2. First we demonstrated that in confluent epithelial monolayers ZO-2 does not travel to the nucleus, as treatment with the PKCε inhibitor peptide does not induce nuclear accumulation of ZO-2. Previously a 19-h turnover rate for ZO-2 was demonstrated in confluent MDCK cells (Gumbiner *et al.*, 1991). This implies that in the 24 h that the experiment lasted, more than half of ZO-2 in the cell was degraded and replaced by newly synthesized ZO-2 that made no trip to the nucleus.

Then we explored whether the bNLSs and SR repeats of ZO-2 regulate the nuclear importation of the protein. With a reporter protein nuclear importation assay we demonstrated that the isolated ZO-2 bNLS-1 is functional but bNLS-2 is not. NLSs are enriched in the basic residues lysine and arginine (Lange *et al.*, 2007), explaining why, due to charge neutralization, the triple phosphomimetic mutation of serines 257, 259, and 261 within bNLS-2 reduces the arrival of ZO-2 to the nucleus in a more significant manner than the single mutation S257E. Loss of functionality by phosphorylation was reported for other NLSs, such as lamin B2 (Hennekes *et al.*, 1993), the transcription factors Jun (Tagawa *et al.*, 1995), Pho4 (Kaffman *et al.*, 1998), Msn2 (Gorner *et al.*, 2002), SWI5/6 (Jans *et al.*, 1995), and basonuclin (Iuchi and Green, 1997), the Ca^{2+}/calmodulin-dependent protein kinase CaM2 (Heist *et al.*, 1998), the tumor suppressor protein adenomatous polyposis coli (Zhang *et al.*, 2001), and the parathyroid hormone–related protein (Lam *et al.*, 1999).

The antibody against ZO-2 pSer257 could not be used for detecting nuclear ZO-2, as it gave strong nuclear speckled staining, even in ZO-2 KD cells. We suspect that this staining was due to the cross-reactivity of the antibody with nuclear factors that contain SR motifs, since BLAST analysis of the sequence [ARHAG(pS)RSRSR] used for generating the antibody reveals bit scores from 29.9 to 26.1 with several splicing factors (SR-rich splicing factors 6 and 12 from the frog *Xenopus tropicalis*; a putative splicing factor from oomycete *Albugo laibachii*; and ASF/SF2 from deer tick, *Ixodes scapularis*), protamine P1 from wallaby, and U2 small nuclear RNA auxiliary factor 2a from zebra fish.

Nevertheless, the antibody ZO-2 pSer257 was very useful, as it allowed us to detect a novel ZO-2 phosphorylation occurring in mature TJs. The phosphorylation of S257 by PKCζ appeared to consolidate immature cell–cell contacts, since it increased with time after the Ca^{2+} switch. These observations agree with results in mouse early embryos, where inhibition of PKCζ blocked the membrane assembly of ZO-2 (Eckert *et al.*, 2005).

We were not able to detect a positive Duolink signal at the plasma membrane when the antibodies against ZO-2 and pSer were used. This might be explained by proposing that in contrast to cancerous cells like HeLa, where positive Duolink signals were found at cell–cell contacts (Rhett *et al.*, 2011), no positive Duolink signals at cell–cell contacts were detected in normal epithelia, possibly due to the tight sealing of their TJs, which impairs proper development of the assay.

By cell fractionation studies, transfection with different ZO-2 segments, and the amino S257A mutant, we were able to demonstrate that *O*-GlcNAcylation of ZO-2 at Ser-257 takes place at the nucleus. The nuclear concentration of ZO-2 observed after transfection with the ZO-2 S257A mutant, as well as the nuclear depletion of ZO-2 present in monolayers treated with PUGNAc, strongly suggested that *O*-GlcNAcylation of S257 promotes nuclear exportation of the protein. In addition, *O*-GlcNAcylation appears to induce proteosomal degradation of nuclear exported ZO-2. These results are in agreement with others showing that polyubiquitination and degradation of the yeast transcriptional repressor Matα2 (Swanson *et al.*, 2001) and of p53 (Freedman and Levine, 1998) require nuclear export and that increasing *O*-GlcNAc levels enhance protein ubiquitination (Guinez *et al.*, 2008).

Transfected SRPK1 exhibits cytoplasmic and nuclear localization, as reported for the endogenous enzyme (Giannakouros *et al.*, 2011). The positive Duolink signal present in the cytoplasm of MDCK cells treated with antibodies against ZO-2 and the FLAG tag of SRPK1 indicates that ZO-2 and SRPK1 associate in the cytoplasm. The concentration of ZO-2 in the nuclei of sparse SRPK1-transfected cells and the distribution of ZO-2 in nuclear speckles triggered by EGF suggest that SRPK1-mediated phosphorylation favors the nuclear import of ZO-2 and its concentration in speckles. These result agree with the observation that SR proteins of *Saccharomyces cerevisiae* are incapable of translocating to the nucleus when SRPK is deleted (Yeakley *et al.*, 1999) and of SF2/ASF human splicing factors whose phosphorylation in the cytoplasm by SRPK1 is required for their transport to the nucleus (Ngo *et al.*, 2005). SRPK1 phosphorylates clusters of SR repeats (Ghosh and Adams, 2011). Hence Ser257 located at a SR motif within bNLS-2, could be a phosphorylation target of SRPK1. We cannot confirm that this phosphorylation takes place at the nucleus, however, as the antibody against ZO-2 pSer257 gives an unspecific nuclear staining, and we do not believe that it occurs in the cytoplasm, since the arrival of ZO-2 at the nucleus is delayed in the mutant S257E.

The inhibition of cell proliferation induced by SRPK1 overexpression might be due to the accumulation of ZO-2 at the nucleus and the nuclear exit of ZASP, since our previous work demonstrated that ZO-2 overexpression inhibits cell proliferation at G0/G1 and decreases CD1 gene transcription and protein level (Huerta *et al.*, 2007; Tapia *et al.*, 2009), whereas ZASP overexpression reverts these effects (Lechuga *et al.*, 2010). These results are in contrast with those obtained upon transfection of a nuclear-directed ZO-2, for which a significant increase in cell proliferation was observed (Traweger *et al.*, 2008). The discrepancy might result from the fact that in the experiment with the nuclear-directed ZO-2, all of the ZO-2 protein synthesized was destined for the nucleus and none for the plasma membrane, provoking an atypical condition in which transepithelial electrical resistance collapsed.

We would like ZO-2 to be considered as a novel SR protein, as it localizes in nuclear speckles (Islas *et al.*, 2002), has 16 SR motifs (Jaramillo *et al.*, 2004), an SRPK-binding motif, and seven putative RNA-binding sites. In addition, ZO-2 shares other characteristics of SR proteins, such as its participation in gene transcription (Huerta *et al.*, 2007) and association with chromatin structure, highlighted by ZO-2 interaction with lamin B (Jaramillo *et al.*, 2004), and with the nuclear matrix protein scaffold attachment factor SAF-B (Traweger *et al.*, 2003).

The fact that EGF signaling through the AKT-SRPK1-SR axis induces the accumulation of ZO-2 at the nucleus suggests that the subcellular localization of the protein responds to physiological clues. In this regard it should be recalled that EGF gains access to its receptor only upon injury or death of cells within the epithelia, as the receptor is present at the basolateral membrane and EGF accumulates at the apical surface (Fukuyama and Shimizu, 1991). Because nuclear ZO-2 has the capacity to block CD1 transcription (Huerta *et al.*, 2007) and the passage of cells from G1 to S (Tapia *et al.*, 2009), finding that EGF triggers the nuclear accumulation of ZO-2 uncovers a novel negative feedback mechanism to down-regulate cell proliferation.

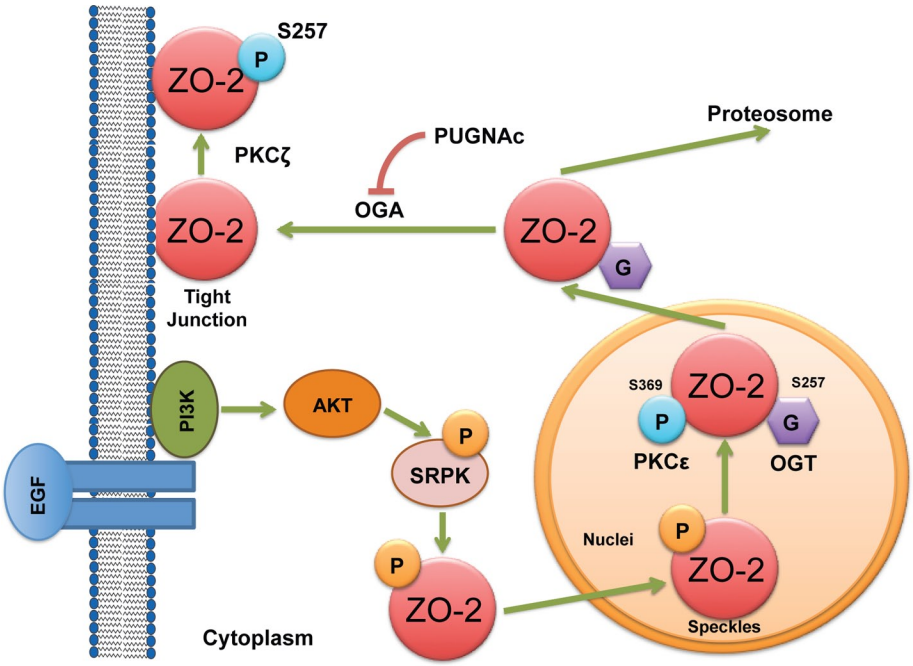

FIGURE 11: Schematic representation of ZO-2 intracellular traffic. In sparse cultures, treatment with EGF activates AKT, which in turn phosphorylates SRPK1. Activated SRPK1 phosphorylates serine residues present at the SR motifs of ZO-2, triggering the importation of the protein to the nucleus. At the nucleus, ZO-2 SR motifs might further become phosphorylated by SRPK1. The phosphorylation at the nucleus of ZO-2 by PKCε at S369 located within NES-1 and the *O*-GlcNAcylation of S257 located within bpNLS-2 induce the nuclear exportation of the protein. Stabilization of *O*-GlcNAcylation with PUGNAc induces proteosomal degradation of the protein. A non–*O*-GlcNAc form of ZO-2 arrive at the TJ that becomes phosphorylated by PKCζ at S257 as the cell–cell contacts mature.

In summary, our results indicate that EGF induces through AKT activation the phosphorylation of SRPK1, which in turn phosphorylates the SR repeats of ZO-2. This phosphorylation provokes ZO-2 entry into the nucleus and accumulation in speckles. ZO-2 arrival at the nucleus is delayed by the phosphomimetic mutation of the serines present within bNLS-2. Stabilizing the *O*-GlcNAcylation of S257 induces ZO-2 departure from the nucleus, followed by proteosomal degradation. At the plasma membrane ZO-2 is not *O*-GlcNAcylated and instead becomes phosphorylated by PKCζ at S257 as TJs mature (Figure 11). This late phosphorylation of S257 is required for the correct development of 3D cultures, as cells transfected with ZO-2 mutant S257A or S257E form aberrant cysts with multiple lumens.

MATERIALS AND METHODS

Cell cultures

Epithelial MDCK cells from the American Type Culture Collection (Manassas, VA; CRL-2936) between the 60th and 90th passages were grown as described previously (Gonzalez-Mariscal *et al.*, 1985). Sparse and confluent cultures were respectively plated at a density of 1×10^5 and 3×10^5 cells/cm^2. MDCK ZO-2 KD were kindly provided by Alan Fanning (University of North Carolina, Chapel Hill, NC) and cultured as previously described (Van Itallie *et al.*, 2009).

Expression plasmids and transfection assays

Full-length canine ZO-2 (fl cZO-2) introduced into the cytomegalovirus expression plasmid pGW1 (pGW1-HA-ZO-2) was kindly provided by Ronald Javier (Baylor College of Medicine, Houston, TX). The cZO-2 amino-terminal segment containing PDZ1, PDZ2, and PDZ3 domains (nucleotides [nt] 398–2165) and the cZO-2 carboxyl-terminal (AP) segment containing the acidic and proline-rich regions (nt 3029–3923) were introduced into the HisMaxB vector as reported previously (Betanzos *et al.*, 2004; Jaramillo *et al.*, 2004). The following point mutants derived from these constructs were made with the QuikChange Multisite-Directed Mutagenesis Kit (200513; Stratagene, Santa Clara, CA), according to the manufacturer's instructions: 1) pGW1-HA–ZO-2: S257E/S259E/S261E, S257A, and S257E and 2) HisMax-ZO-2-amino S257A. SRPK1 was cloned into the FLAG-CMV2 vector as previously described (Nikolakaki *et al.*, 2001) pFLAG-CMV-2-BAP was used as control vector (E7033, Sigma-Aldrich, St. Louis, MO). Transfections of these plasmids and derived mutants were done with Lipofectamine 2000 (11668-019; Invitrogen, Carlsbad, CA) according to the manufacturer's instructions. The siRNA for canine SRPK1 was custom synthesized by Thermo Scientific Dharmacon (Lafayette, CO) and transfected into MDCK cells with Lipofectamine RNAiMAX (13778-150; Life Technologies, Grand Island, NY).

Immunofluorescence

Monolayers grown on glass coverslips were fixed with 2% (wt/vol) paraformaldehyde in phosphate-buffered saline (PBS), pH 7.4, and permeabilized for 10 min with 0.5% (vol/vol) Triton X-100 in PBS. Cells were washed five times with PBS and then blocked for 30 min with 1% (wt/vol) bovine serum albumin (immunoglobulin [Ig] free; 1331-A; Research Organics, Cleveland, OH). The monolayers were incubated overnight at 4°C with rabbit polyclonal anti–ZO-2 (71-1400, dilution 1:100; Invitrogen) and a custom-made anti–p-Ser257 of ZO-2 (dilution 1:50; ProSci, Poway, CA) or mouse monoclonals against ovalbumin (A6075, dilution 1:50; Sigma-Aldrich), SRPK1 (ab58002, dilution 1:100; Abcam, Cambridge, MA), and FLAG (F3165, dilution 1:50; Sigma-Aldrich). After 5× washing with PBS, the coverslips were incubated for 1 h at room temperature with Alexa Fluor 488–coupled goat anti-rabbit (A11008, dilution 1:300; Life Technologies) and goat anti mouse (A11001, dilution 1:300; Life Technologies) or Alexa Fluor 594–coupled goat anti-mouse (A1105, dilution 1:300; Life Technologies) antibodies. After 3× washing, the monolayers were mounted with the antifade reagent Vectashield (H-1000; Vector Laboratories, Burlingame, CA). The fluorescence of the monolayers was examined using an SP2 confocal microscope (Leica, Wetzlar, Germany) with argon and helium–neon lasers and Leica confocal software.

Analysis of the nuclear recruitment of ZO-2

At different time points taken after transfecting MDCK cells with HA–ZO-2 or the mutant S257A or S257E, the cells were fixed and processed for immunofluorescence with an antibody against HA. The observations were initiated 6 h after transfection (time 0). In all experimental conditions, at each time point, the subcellular distribution patterns of HA–ZO-2 were analyzed in 100 transfected cells

observed in an Eclipse E600 microscope (Nikon, Tokyo, Japan) by using a 63× objective lens. The nuclear recruitment index refers to the percentage of transfected cells exhibiting nuclear stain and is integrated by cells displaying nuclear distribution in any of the following patterns: only nuclear, membrane and nuclear, cytoplasm and nuclear, and cytoplasm, nuclear, and membrane, as previously described (Chamorro *et al.*, 2009)

Cyst formation

MDCK cells were transfected with Lipofectamine 2000 with ZO-2 WT or the mutant S257A or S257E. One day later 3×10^6 cells were trypsinized, resuspended in 30 µl of DMEM, mixed with 20 µl of Matrigel, plated on top of a Transwell insert (polycarbonate filter, 6.5 mm diameter, 0.4-µm pores; catalog no. 3414; Corning, Tewksbury MA), placed inside a 24-multiwell plate containing DMEM, and incubated for 1 h at 37°C in an air–5% CO_2 atmosphere. Then the upper chamber of the Transwell was bathed with 100 µl of cDMEM (complete DMEM) and left in the incubator for additional 8 d, replenishing the culture media with fresh cDMEM every third day. The cultures were then fixed with 2% paraformaldehyde, permeabilized with 0.5% Triton X-100 in PBS, and processed for immunofluorescence in the Transwell insert by overnight incubation with specific antibodies against ZO-2 and gp135/podocalyxin (a kind gift of George Ojakian, SUNY Downstate Medical Center, Brooklyn, NY). The Transwells were next incubated overnight with the secondary antibodies Alexa Fluor 594 anti-mouse and Alexa Fluor 488 anti-rabbit. After six washes with PBS, the Transwell was inverted and the filter detached with a cutter. Then the Matrigel matrix containing the cysts was pulled away from the underlying filter by pushing the gelatinous matrix with a spatula and placing it upon a slide, where it was covered with mounting media with 4′,6-diamidino-2-phenylindole (DAPI; Duo82040; Sigma-Aldrich) and a coverslip and was observed in the confocal microscope.

Reporter protein nuclear importation assay

To analyze whether the putative bNLSs in canine ZO-2 sequence are functional, we designed a reporter protein nuclear importation assay. For this purpose, we chemically coupled synthetic peptides homologous to ZO-2 bNLSs (bNLS-1: $_{83}$RKSGKIAAIVVKRPRK$_{98}$ and bNLS-2: $_{246}$RRTQPDARHAGSRSRSR$_{262}$) to the reporter protein ovalbumin (bNLS-1-OVA and bNLS-2-OVA; customized synthesis and coupling by Invitrogen) at a ratio of one bNLS peptide per ovalbumin molecule. Ovalbumin was selected as reporter protein due to its lack of NLS and NES and 45 kDa size, which does not allow passive diffusion through the nuclear pore complex. Rhodamine-conjugated albumin was used as negative control. For the assay, the cytoplasm of live MDCK cells was microinjected with a solution containing 7 µl of solution A (120 mM KCl, 5 mM NaCl, 1 mM $MgCl_2$, 5 mM ethylene glycol tetraacetic acid–K^+, and 10 mM 4-(2-hydroxyethyl)-1-piperazineethanesulfonic acid, pH 7.4), 1 µl of rhodaminated albumin (A23016, 0.5 mg/ml; Invitrogen), and 2 µl of bNLS-1-OVA or bNLS-2-OVA. Microinjection was performed using an IM 300 apparatus (Narishige, Tokyo, Japan) with glass micropipettes (Kimax 34500; Kimble Chase, Vineland, NJ) with tip diameter of ~0.2 µm, equivalent to an electrical resistance of ~10 mΩ, made with a horizontal Brown/Flaming puller (Sutter p87; Sutter Instrument, Novato, CA). After backfilling, the pipettes were attached to a holder connected to a piezoelectric micromanipulator (PCS500; Burleigh, New York, NY). The microinjection was performed on the cytoplasm of sparse cells plated 8–12 h before on glass coverslips and was verified by epifluorescence observation of the injected rhodaminated albumin in an inverted microscope (Diaphot 200; Nikon). After 2 h of incubation at 37°C the cells were fixed, permeabilized, and processed for immunofluorescence.

ZO-2 immunoprecipitation

ZO-2 was immunoprecipitated from sparse MDCK cells with antibodies against ZO-2, HA (H9658; Sigma-Aldrich), or p-Ser257 ZO-2 as described by Tapia *et al.* (2009). ZO-2 immunoprecipitation from the nuclear and membrane fractions of MDCK cells was done as described by Chamorro *et al.* (2009).

Cellular lysates, SDS–PAGE, and Western blot

MDCK cells were lysed under gentle rotation for 15 min at 4°C with radioimmunoprecipitation assay (RIPA) buffer (40 mM Tris-HCl, pH 7.6, 150 mM NaCl, 2 mM EDTA, pH 8.0, 10% [vol/vol] glycerol, 1% [vol/vol] Triton X-100, 0.5% [wt/vol] sodium deoxycholate, 0.2% [wt/vol] SDS, and 1 mM phenylmethylsulfonyl fluoride) containing the protease inhibitor cocktail Complete (04906837001; Roche, Indianapolis, IN). Subsequently the lysates were sonicated three times for 30 s each in a high-intensity ultrasonic processor (Vibra-Cell; Sonics and Materials, Danbury, CT). The proteins in the cellular extracts were quantified, and the samples were diluted (1:5) in sample buffer (125 mM Tris-HCl, 4% [wt/vol] SDS, 20% [vol/vol] glycerol, 10% [vol/vol] 2-mercaptoethanol, pH 6.8), run in 12% polyacrylamide gels, and transferred to polyvinylidene difluoride membranes (GE Healthcare, Little Chalfont, United Kingdom). The following primary antibodies were used: rabbit polyclonal anti–ZO-2 (71-1400, dilution 1:1000; Invitrogen, Grand Island, NY) and mouse monoclonals anti-HA (H9658, dilution 1:1000; Sigma-Aldrich,), anti-Xpress (R910-25, dilution 1:5000; Life Technologies), anti-FLAG (F1304, dilution 1:1000; Sigma-Aldrich), anti *O*-GlcNAc (MO1038, dilution 1:1000; Thermo Scientific, Waltham, MA), anti P-Ser (P3430, dilution 1:200; Sigma-Aldrich); anti–β_1 subunit of the Na^+-K^+-ATPase (dilution 1:200; kindly donated by Michael Caplan, Yale University, New Haven, CT), anti–lamin B1 (33-2000, dilution 1:100; Life Technologies), and anti-actin (dilution 1:2000; kindly donated by Manuel Hernández, Center for Research and Advanced Studies, Mexico City, Mexico). Peroxidase-conjugated goat IgG against rabbit IgG (62-6120, dilution 1:3000; Zymed Laboratories, South San Francisco, CA) and mouse IgG (62-6520, dilution 1:3000; Zymed Laboratories) were used as secondary antibodies, followed by Immobilon chemiluminescence detection (WBKLS0500; Millipore, Billerica, MA).

For the mobility shift detection assay of phosphorylated proteins, phosphate affinity SDS–PAGE was done with the acrylamide-pendant Phos-tag ligand (AAL-107; Wako Pure Chemical Industries, Richmond, VA) according to the manufacturer's instructions.

Alkaline phosphatase treatment

Cells were harvested in ice-cold PBS, pelleted by centrifugation, and resuspended in NEB Buffer 3 (100 mM NaCl, 50 mM Tris-HCl, 10 mM $MgCl_2$, and 1 mM dithiothreitol, pH 7.9; B7003S, New England BioLabs, Ipswich, MA). Then the cells were sonicated and incubated for 60 min at 37°C with the 20 U of calf intestine alkaline phosphatase (M0290S; New England BioLabs). Samples were then processed for Western blot.

Protein purification

Sparse cultures of MDCK cells were transfected with HisMax-ZO-2-NH_2 and HisMax-ZO-2-AP. After 24 h the cells were lysed with RIPA buffer and the lysates passed through HisTrap FF affinity

chromatography columns (17-5319-01; GE Healthcare, Pittsburgh, PA) as indicated by the manufacturer. Purified fractions were resolved by SDS–PAGE and processed by Western blot.

Duolink in situ proximity ligation assay

The Duolink in situ proximity ligation assay (92101; Olink Bioscience, Uppsala, Sweden) was done according to the manufacturer's instructions. Cell borders were stained with rat anti–E-cadherin antibody (U3254, dilution 1:100; Sigma-Aldrich), followed by anti-rat antibody coupled to FITC (F1763, dilution 1:100; Sigma-Aldrich).

Cell proliferation assay

A Cell Counting Kit-8 (CK0401; Dojindo, Rockville, MD) was used to measure cell proliferation.

Drugs

The PKCε permeable inhibitor peptide εv1-2 (CFNGLLKIKI; kindly provided by Daria Mochly-Rosen, Stanford University, Stanford, CA) was dissolved in water as a stock at a concentration of 1 mM and used at a final concentration of 1 μM. The PKCε permeable activating peptide ψεRACK (HDAPIGYD; kindly provided by Daria Mochly-Rosen) was dissolved in water as a stock at a concentration of 1 mM and used at a final concentration of 1 μM. Myristoylated PKCζ pseudosubstrate (539624; EMD Millipore, Darmstadt, Germany) was prepared as a 2 μg/ml stock in water and used at final concentration of 50 μM. Gö6850 (203290; EMD Millipore) was prepared as a 6 mM stock in dimethyl sulfoxide (DMSO) and used at final concentrations of 2 and 6 mM. PUGNAc (A7229; Sigma-Aldrich) was prepared as a 100 mM stock in water and used at final concentration of 100 μM. MG132 (C2211; Sigma-Aldrich) was prepared as a 20 mM stock in DMSO and used at final concentration of 50 μM. Triciribine (124012; EMD Millipore) was prepared as a 30 mM stock in DMSO and used at final concentration of 30 μM. EGF (E9644; Sigma-Aldrich) was prepared as a 10 μM stock in water and used at final concentration of 100 nM.

ACKNOWLEDGMENTS

This work was supported by Mexican National Council of Science and Technology (Conacyt) Grant 98448. M.Q. was a recipient of a doctoral fellowship from Conacyt (209822).

REFERENCES

Adam SA, Nakagawa T, Swanson MS, Woodruff TK, Dreyfuss G (1986). mRNA polyadenylate-binding protein: gene isolation and sequencing and identification of a ribonucleoprotein consensus sequence. Mol Cell Biol 6, 2932–2943.

Betanzos A, Huerta M, Lopez-Bayghen E, Azuara E, Amerena J, Gonzalez-Mariscal L (2004). The tight junction protein ZO-2 associates with Jun, Fos and C/EBP transcription factors in epithelial cells. Exp Cell Res 292, 51–66.

Boucher L, Ouzounis CA, Enright AJ, Blencowe BJ (2001). A genome-wide survey of RS domain proteins. RNA 7, 1693–1701.

Carlton VE *et al*. (2003). Complex inheritance of familial hypercholanemia with associated mutations in TJP2 and BAAT. Nat Genet 34, 91–96.

Chamorro D *et al*. (2009). Phosphorylation of zona occludens-2 by protein kinase C epsilon regulates its nuclear exportation. Mol Biol Cell 20, 4120–4129.

Dreyfuss G, Swanson MS, Pinol-Roma S (1988). Heterogeneous nuclear ribonucleoprotein particles and the pathway of mRNA formation. Trends in Biochem Sci 13, 86–91.

Eckert JJ, McCallum A, Mears A, Rumsby MG, Cameron IT, Fleming TP (2005). Relative contribution of cell contact pattern, specific PKC isoforms and gap junctional communication in tight junction assembly in the mouse early embryo. Dev Biol 288, 234–247.

Elia N, Lippincott-Schwartz J (2009). Culturing MDCK cells in three dimensions for analyzing intracellular dynamics. Curr Protoc Cell Biol Chapter 4, Unit 4.22.

Fanning AS, Anderson JM (2009). Zonula occludens-1 and -2 are cytosolic scaffolds that regulate the assembly of cellular junctions. Ann NY Acad Sci 1165, 113–120.

Freedman DA, Levine AJ (1998). Nuclear export is required for degradation of endogenous p53 by MDM2 and human papillomavirus E6. Mol Cell Biol 18, 7288–7293.

Fukuyama R, Shimizu N (1991). Detection of epidermal growth factor receptors and E-cadherins in the basolateral membrane of A431 cells by laser scanning fluorescence microscopy. Jpn J Cancer Res 82, 8–11.

Ghosh G, Adams JA (2011). Phosphorylation mechanism and structure of serine-arginine protein kinases. FEBS J 278, 587–597.

Giannakouros T, Nikolakaki E, Mylonis I, Georgatsou E (2011). Serine-arginine protein kinases: a small protein kinase family with a large cellular presence. FEBS J 278, 570–586.

Gonzalez-Mariscal L, Betanzos A, Nava P, Jaramillo BE (2003). Tight junction proteins. Prog Biophys Mol Biol 81, 1–44.

Gonzalez-Mariscal L, Chavez de Ramirez B, Cereijido M (1985). Tight junction formation in cultured epithelial cells (MDCK). J Membrane Biol 86, 113–125.

Gonzalez-Mariscal L, Ponce A, Alarcon L, Jaramillo BE (2006). The tight junction protein ZO-2 has several functional nuclear export signals. Exp Cell Res 312, 3323–3335.

Gonzalez-Mariscal L, Quiros M, Diaz-Coranguez M (2011). ZO proteins and redox-dependent processes. Antioxid Redox Signal 15, 1235–1253.

Gorner W, Durchschlag E, Wolf J, Brown EL, Ammerer G, Ruis H, Schuller C (2002). Acute glucose starvation activates the nuclear localization signal of a stress-specific yeast transcription factor. EMBO J 21, 135–144.

Guinez C, Mir AM, Dehennaut V, Cacan R, Harduin-Lepers A, Michalski JC, Lefebvre T (2008). Protein ubiquitination is modulated by *O*-GlcNAc glycosylation. FASEB J 22, 2901–2911.

Gumbiner B, Lowenkopf T, Apatira D (1991). Identification of a 160-kDa polypeptide that binds to the tight junction protein ZO-1. Proc Natl Acad Sci USA 88, 3460–3464.

Haltiwanger RS, Grove K, Philipsberg GA (1998). Modulation of O-linked N-acetylglucosamine levels on nuclear and cytoplasmic proteins in vivo using the peptide *O*-GlcNAc-beta-N-acetylglucosaminidase inhibitor O-(2-acetamido-2-deoxy-D-glucopyranosylidene)amino-N-phenylcarbamate. J Biol Chem 273, 3611–3617.

Hart GW, Housley MP, Slawson C (2007). Cycling of O-linked beta-N-acetylglucosamine on nucleocytoplasmic proteins. Nature 446, 1017–1022.

Hedley ML, Amrein H, Maniatis T (1995). An amino acid sequence motif sufficient for subnuclear localization of an arginine/serine-rich splicing factor. Proc Natl Acad Sci USA 92, 11524–11528.

Heist EK, Srinivasan M, Schulman H (1998). Phosphorylation at the nuclear localization signal of Ca2+/calmodulin-dependent protein kinase II blocks its nuclear targeting. J Biol Chem 273, 19763–19771.

Hennekes H, Peter M, Weber K, Nigg EA (1993). Phosphorylation on protein kinase C sites inhibits nuclear import of lamin B2. J Cell Biol 120, 1293–1304.

Hernandez S, Chavez Munguia B, Gonzalez-Mariscal L (2007). ZO-2 silencing in epithelial cells perturbs the gate and fence function of tight junctions and leads to an atypical monolayer architecture. Exp Cell Res 313, 1533–1547.

Huang HY, Li R, Sun Q, Wang J, Zhou P, Han H, Zhang WH (2002). LIM protein KyoT2 interacts with human tight junction protein ZO-2-i3 [in Chinese]. Yi Chuan Xue Bao 29, 953–958.

Huerta M, Munoz R, Tapia R, Soto-Reyes E, Ramirez L, Recillas-Targa F, Gonzalez-Mariscal L, Lopez-Bayghen E (2007). Cyclin D1 is transcriptionally down-regulated by ZO-2 via an E box and the transcription factor c-Myc. Mol Biol Cell 18, 4826–4836.

Inagaki K, Begley R, Ikeno F, Mochly-Rosen D (2005). Cardioprotection by epsilon-protein kinase C activation from ischemia: continuous delivery and antiarrhythmic effect of an epsilon-protein kinase C-activating peptide. Circulation 111, 44–50.

Islas S, Vega J, Ponce L, Gonzalez-Mariscal L (2002). Nuclear localization of the tight junction protein ZO-2 in epithelial cells. Exp Cell Res 274, 138–148.

Iuchi S, Green H (1997). Nuclear localization of basonuclin in human keratinocytes and the role of phosphorylation. Proc Natl Acad Sci USA 94, 7948–7953.

Jans DA, Moll T, Nasmyth K, Jans P (1995). Cyclin-dependent kinase site-regulated signal-dependent nuclear localization of the SW15 yeast transcription factor in mammalian cells. J Biol Chem 270, 17064–17067.

Jaramillo BE, Ponce A, Moreno J, Betanzos A, Huerta M, Lopez-Bayghen E, Gonzalez-Mariscal L (2004). Characterization of the tight junction

protein ZO-2 localized at the nucleus of epithelial cells. Exp Cell Res 297, 247–258.
Jesaitis LA, Goodenough DA (1994). Molecular characterization and tissue distribution of ZO-2, a tight junction protein homologous to ZO-1 and the *Drosophila* discs-large tumor suppressor protein. J Cell Biol 124, 949–961.
Kaffman A, Rank NM, O'Shea EK (1998). Phosphorylation regulates association of the transcription factor Pho4 with its import receptor Pse1/Kap121. Genes Dev 12, 2673–2683.
Kausalya PJ, Phua DC, Hunziker W (2004). Association of ARVCF with zonula occludens (ZO)-1 and ZO-2: binding to PDZ-domain proteins and cell-cell adhesion regulate plasma membrane and nuclear localization of ARVCF. Mol Biol Cell 15, 5503–5515.
Lai MC, Teh BH, Tarn WY (1999). A human papillomavirus E2 transcriptional activator. The interactions with cellular splicing factors and potential function in pre-mRNA processing. J Biol Chem 274, 11832–11841.
Lam MH, House CM, Tiganis T, Mitchelhill KI, Sarcevic B, Cures A, Ramsay R, Kemp BE, Martin TJ, Gillespie MT (1999). Phosphorylation at the cyclin-dependent kinases site (Thr85) of parathyroid hormone-related protein negatively regulates its nuclear localization. J Biol Chem 274, 18559–18566.
Lange A, Mills RE, Lange CJ, Stewart M, Devine SE, Corbett AH (2007). Classical nuclear localization signals: definition, function, and interaction with importin alpha. J Biol Chem 282, 5101–5105.
Lechuga S, Alarcon L, Solano J, Huerta M, Lopez-Bayghen E, Gonzalez-Mariscal L (2010). Identification of ZASP, a novel protein associated to zona occludens-2. Exp Cell Res 316, 3124–3139.
Lee DH, Goldberg AL (1998). Proteasome inhibitors: valuable new tools for cell biologists. Trends Cell Biol 8, 397–403.
Liedtke CM, Yun CH, Kyle N, Wang D (2002). Protein kinase C epsilon-dependent regulation of cystic fibrosis transmembrane regulator involves binding to a receptor for activated C kinase (RACK1) and RACK1 binding to Na+/H+ exchange regulatory factor. J Biol Chem 277, 22925–22933.
Macara IG (2001). Transport into and out of the nucleus. Microbiol Mol Biol Rev 65, 570–594.
Mandel LJ, Bacallao R, Zampighi G (1993). Uncoupling of the molecular "fence" and paracellular "gate" functions in epithelial tight junctions. Nature 361, 552–555.
Mihlan S, Reiss C, Thalheimer P, Herterich S, Gaetzner S, Kremerskothen J, Pavenstadt HJ, Lewandrowski U, Sickmann A, Butt E (2012). Nuclear import of LASP-1 is regulated by phosphorylation and dynamic protein-protein interactions. Oncogene 32, 2107–2113.
Ngo JC, Chakrabarti S, Ding JH, Velazquez-Dones A, Nolen B, Aubol BE, Adams JA, Fu XD, Ghosh G (2005). Interplay between SRPK and Clk/Sty kinases in phosphorylation of the splicing factor ASF/SF2 is regulated by a docking motif in ASF/SF2. Mol Cell 20, 77–89.
Nikolakaki E, Kohen R, Hartmann AM, Stamm S, Georgatsou E, Giannakouros T (2001). Cloning and characterization of an alternatively spliced form of SR protein kinase 1 that interacts specifically with scaffold attachment factor-B. J Biol Chem 276, 40175–40182.
Oka T *et al*. (2010). Functional complexes betweeNYAP2 and ZO-2 are PDZ domain-dependent, and regulate YAP2 nuclear localization and signalling. Biochem J 432, 461–472.
Puigserver P, Wu Z, Park CW, Graves R, Wright M, Spiegelman BM (1998). A cold-inducible coactivator of nuclear receptors linked to adaptive thermogenesis. Cell 92, 829–839.
Rhett JM, Jourdan J, Gourdie RG (2011). Connexin 43 connexon to gap junction transition is regulated by zonula occludens-1. Mol Biol Cell 22, 1516–1528.
Song JC, Hanson CM, Tsai V, Farokhzad OC, Lotz M, Matthews JB (2001). Regulation of epithelial transport and barrier function by distinct protein kinase C isoforms. Am J Physiol Cell Physiol 281, C649–C661.
Srikanth B, Vaidya MM, Kalraiya RD (2010). *O*-GlcNAcylation determines the solubility, filament organization, and stability of keratins 8 and 18. J Biol Chem 285, 34062–34071.
Standaert ML, Galloway L, Karnam P, Bandyopadhyay G, Moscat J, Farese RV (1997). Protein kinase C-zeta as a downstream effector of phosphatidylinositol 3-kinase during insulin stimulation in rat adipocytes. Potential role in glucose transport. J Biol Chem 272, 30075–30082.
Swanson R, Locher M, Hochstrasser M (2001). A conserved ubiquitin ligase of the nuclear envelope/endoplasmic reticulum that functions in both ER-associated and Matalpha2 repressor degradation. Genes Dev 15, 2660–2674.
Tagawa T, Kuroki T, Vogt PK, Chida K (1995). The cell cycle-dependent nuclear import of v-Jun is regulated by phosphorylation of a serine adjacent to the nuclear localization signal. J Cell Biol 130, 255–263.
Tapia R, Huerta M, Islas S, Avila-Flores A, Lopez-Bayghen E, Weiske J, Huber O, Gonzalez-Mariscal L (2009). Zona occludens-2 inhibits cyclin D1 expression and cell proliferation and exhibits changes in localization along the cell cycle. Mol Biol Cell 20, 1102–1117.
Traweger A, Fuchs R, Krizbai IA, Weiger TM, Bauer HC, Bauer H (2003). The tight junction protein ZO-2 localizes to the nucleus and interacts with the heterogeneous nuclear ribonucleoprotein scaffold attachment factor-B. J Biol Chem 278, 2692–2700.
Traweger A, Lehner C, Farkas A, Krizbai IA, Tempfer H, Klement E, Guenther B, Bauer HC, Bauer H (2008). Nuclear zonula occludens-2 alters gene expression and junctional stability in epithelial and endothelial cells. Differentiation 76, 99–106.
Tsukita S, Katsuno T, Yamazaki Y, Umeda K, Tamura A, Tsukita S (2009). Roles of ZO-1 and ZO-2 in establishment of the belt-like adherens and tight junctions with paracellular permselective barrier function. Ann NY Acad Sci 1165, 44–52.
Valcarcel J, Green MR (1996). The SR protein family: pleiotropic functions in pre-mRNA splicing. Trends Biochem Sci 21, 296–301.
Van Itallie CM, Fanning AS, Bridges A, Anderson JM (2009). ZO-1 stabilizes the tight junction solute barrier through coupling to the perijunctional cytoskeleton. Mol Biol Cell 20, 3930–3940.
Walsh T *et al*. (2010). Genomic duplication and overexpression of TJP2/ZO-2 leads to altered expression of apoptosis genes in progressive nonsyndromic hearing loss DFNA51. Am J Hum Genet 87, 101–109.
Xu J, Anuar F, Ali SM, Ng MY, Phua DC, Hunziker W (2009). Zona occludens-2 is critical for blood-testis barrier integrity and male fertility. Mol Biol Cell 20, 4268–4277.
Xu J, Kausalya PJ, Phua DC, Ali SM, Hossain Z, Hunziker W (2008). Early embryonic lethality of mice lacking ZO-2, but Not ZO-3, reveals critical and nonredundant roles for individual zonula occludens proteins in mammalian development. Mol Cell Biol 28, 1669–1678.
Yang L *et al*. (2004). Akt/protein kinase B signaling inhibitor-2, a selective small molecule inhibitor of Akt signaling with antitumor activity in cancer cells overexpressing Akt. Cancer Res 64, 4394–4399.
Yeakley JM, Tronchere H, Olesen J, Dyck JA, Wang HY, Fu XD (1999). Phosphorylation regulates in vivo interaction and molecular targeting of serine/arginine-rich pre-mRNA splicing factors. J Cell Biol 145, 447–455.
Zhang F, White RL, Neufeld KL (2001). Cell density and phosphorylation control the subcellular localization of adenomatous polyposis coli protein. Mol Cell Biol 21, 8143–8156.
Zhou Z *et al*. (2012). The Akt-SRPK-SR axis constitutes a major pathway in transducing EGF signaling to regulate alternative splicing in the nucleus. Mol Cell 47, 422–433.